5-2012

EVIDENCE OF HUMAN ENDOGENOUS RETROVIRUS K INVOLVEMENT IN HUMAN CANCER

Joshua B. Plummer

EVIDENCE OF HUMAN ENDOGENOUS RETROVIRUS K

INVOLVEMENT IN HUMAN CANCER

by

Joshua B. Plummer, B.S.

APPROVED:

_____
Feng Wang-Johanning, M.D., Ph.D.
Supervisory Professor

_____
Gary Johanning, Ph.D.

_____
Rick Finch, Ph.D.

_____
Mark McArthur, D.V.M.

_____
Dean Tang, Ph.D.

_____
Victoria Knutson, Ph.D.

APPROVED:

_____
Dean, The University of Texas
Graduate School of Biomedical Sciences

EVIDENCE OF HUMAN ENDOGENOUS RETROVIRUS K INVOLVEMENT IN HUMAN CANCER

A

THESIS

Presented to the Faculty of
The University of Texas
Health Science Center at Houston
and
The University of Texas
M. D. Anderson Cancer Center
Graduate School of Biomedical Sciences
in Partial Fulfillment

of the Requirements

for the Degree of

MASTER OF SCIENCE

by

Joshua B. Plummer, B.S.

Houston, Texas

May 2012

Acknowledgements

I would like to thank my supervisor Dr. Feng Wang-Johanning for her continuous guidance, patience, and support.

I also would like to thank my supervisory committee Dr. Rick Finch, Dr. Mark McArthur, Dr. Gary Johanning, Dr. Dean Tang, and Dr. Victoria Knutson for their insight, support, and commitment to my project.

In addition, Dr. Wang-Johanning's lab staff Kiera Rycaj, Ming Li, and Jeremy Garza were a great help and their support is much appreciated.

Dr. Dwight Romanovicz's teaching, insight, and technical excellence in the arena of electron microscopy were invaluable assets to our project.

Dr. Mark Bedford's generosity in letting us use his facilities and Biacore equipment was crucial to our ability to do those studies and we owe him a great deal of gratitude.

Dr. Collene Jeter's time and assistance was crucial in enabling us to complete the portions of the project involving confocal microscopy and we would like to thank her for all of her efforts.

Dr. Larry Williams's insight with respect to data analysis was of great assistance and is also very much appreciated.

EVIDENCE OF HUMAN ENDOGENOUS RETROVIRUS K INVOLVEMENT IN HUMAN CANCER

Publication No._____

Joshua B. Plummer, B.S.

Supervisory Professor: Feng Wang-Johanning, M.D., Ph.D.

Many lines of clinical and experimental evidence indicate a viral role in carcinogenesis (1-6). Our access to patient plasma, serum, and tissue samples from invasive breast cancer (N=19), ductal carcinoma *in situ* (N=13), malignant ovarian cancer (N=12), and benign ovarian tumors (N=9), via IRB-approved and informed consent protocols through M.D. Anderson Cancer Center, as well as normal donor plasmas purchased from Gulf Coast Regional Blood Center (N=6), has allowed us to survey primary patient blood and tissue samples, healthy donor blood from the general population, as well as commercially available human cell lines for the presence of human endogenous retrovirus K (HERV-K) Env viral RNA (vRNA), protein, and viral particles. We hypothesize that HERV-K proteins are tumor-associated antigens and as such can be profiled and targeted in patients for diagnostic and therapeutic purposes. To test this hypothesis, we employed isopycnic ultracentrifugation, a microplate-based reverse transcriptase enzyme activity assay, reverse transcription – polymerase chain reaction (RT-PCR), cDNA sequencing, SDS-PAGE and western blotting, immunofluorescent staining, confocal microscopy, and transmission electron microscopy to evaluate

HERV-K activation in cancer. Data from large numbers of patients tested by reverse transcriptase activity assay were analyzed statistically by t-test to determine the potential use of this assay as a diagnostic tool for cancer.

Significant reverse transcriptase enzyme activity was detected in 75% of ovarian cancer patients, 53.8% of ductal carcinoma *in situ* patient, and 42.1% of invasive breast cancer patient samples. Only 11.1% of benign ovarian patient and 16.7% of normal donor samples tested positive. HERV-K Env vRNA, or Env SU were detected in the majority of cancer types screened, as demonstrated by the results shown herein, and were largely absent in normal controls. These findings support our hypothesis that the presence of HERV-K in patient blood circulation is an indicator of cancer or pre-malignancy *in vivo*, that the presence of HERV-K Env on tumor cell surfaces is indicative of malignant phenotype, and that HERV-K Env is a tumor-associated antigen useful not only as a diagnostic screening tool to predict patient disease status, but also as an exploitable therapeutic target for various novel antibody-based immunotherapies.

Table of Contents

LIST OF ILLUSTRATIONS

LIST OF TABLES

ABBREVIATIONS

Acc	patient accrual number
ACUF	Animal Care and Use Form
AuNP	gold nanoparticle
BSA	bovine serum albumin
CASE	carboxylic acid succinimidyl ester
CFCA	calibration-free concentration analysis
DAPI	4',6-diamidino-2-phenylindole
EDC	1-ethyl-3-(3-dimethylaminopropyl) carbodiimide
EDTA	ethylenediaminetetraacetic acid
Env	Envelope protein
FBS	fetal bovine serum
FPLC	fast protein liquid chromatography
Gag	group antigen
GST	glutathione-S-transferase
HBS	HEPES-buffered saline pH 7.5
HBS-EP	HEPES-buffered saline+3mM EDTA+0.005% Tween 20
HEPES	4-(2-Hydroxyethyl) piperazine-1-ethanesulfonic acid
HERV-K	Human Endogenous Retrovirus K family
HRP	horseradish peroxidase
IACUC	Institutional Animal Care and Use Committee
IgG	gamma globulin
ip	intraperitoneal

iv	intravenous
kb	kilobase
K_D	thermodynamic affinity constant
kDa	kilodalton
kv	kilovolt
LTR	long tandem repeat
M	molar
mAb	monoclonal antibody
μg	microgram
mRNA	messenger ribonucleic acid
MWCO	molecular weight cutoff
NHS	N-hydroxyl succinamide
OsO_4-KFeCN	osmium tetroxide + potassium ferrocyanide
PBS	phosphate-buffered saline, pH 7.4
PVDF	polyvinylidene fluoride
RFU	relative fluorescence unit
RT	Reverse transcriptase
RT-PCR	reverse transcription-polymerase chain reaction
RU	resonance units
sc	subcutaneous
SDS-PAGE	sodium dodecyl sulfate - polyacrylamide gel electrophoresis
SFCA	surfactant-free cellulose acetate

SPR	surface plasmon resonance
SU	surface domain
TAE	tris-acetate-EDTA buffer
TBS	tris-buffered saline, pH 7.6
TEM	transmission electron microscopy
TM	transmembrane domain
tRNA	transfer ribonucleic acid
UA	uranyl acetate
Vhr	volt-hour
vRNA	viral ribonucleic acid
xg	times gravity (G-force)

Chapter 1 Introduction

For over a century there has been an association between viruses and cancer. Peyton Rous, building on the work of Bang and Ellerman, announced the isolation of a filterable cell-free lysate from solid tumor that was capable of transmitting those solid tumors in chickens in 1910 (1). Mammalian tumor viruses were first discovered by RE Shope in 1933, with Shope papilloma virus in rabbits (2). As early as 1936, the physiological effects of mouse mammary tumor virus had been witnessed and described by JJ Bittner, though he never directly implicated a viral agent in his preliminary report (3). The discovery of viral proto-oncogenes *src*, *myc*, *ras*, and many others was ground-breaking as their existence helped elucidate a mechanism for viral transformation of normal tissues into neoplasia (4). Viruses that have been directly implicated in human cancer include Epstein-Barr virus (EBV) in Burkitt's and Hodgkin's lymphoma as well as nasopharangeal carcinoma, human papilloma virus (HPV16 and 18) in cervical cancer, human herpesvirus (HHV-8) in Kaposi's sarcoma, and human T-cell lymphotrophic virus (HTLV-1) in adult T-cell leukemia and lymphoma (5,6).

One emerging viral instigator of cancer, with growing evidence accumulating from studies of a variety of human cancers done in our lab and others, is a group of proteins encoded by genetic artifacts of human endogenous retrovirus (HERV). The upcoming sections will focus on the structure, organization, and phylogeny of HERV-K as well as its role in human cancer.

1.1 Human endogenous retrovirus (HERV)

1.1.1 Origins of HERVs in the human genome

Integration of HERVs into the human genome has yielded stable remnants of retroviruses that have been determined to constitute nearly 8% of the human genome (7). Within these integrated elements can be found consensus retroviral *gag*, *pol* (coding for protease and reverse transcriptase), and *env* (both surface and transmembrane domains) coding regions. Most families of HERV are degenerate in that their coding regions lack fidelity due to deletions and nonsense mutations and therefore do not typically produce functional proteins. In the host, epigenetic regulation is also at work here, modulating the expression levels of HERV genes through engagement of GC boxes found in the LTRs flanking viral coding regions (8, 9). The K family of HERV, named for its use of the lysine tRNA as a primer in replication, is evolutionarily related to type 2 betaretroviruses. HERV-K has been reported to be the youngest of all identified HERV families and insertions of HERV-K genes with open reading frames can be found across multiple chromosomes in the human genome (11). Expression of human endogenous retroviral proteins has been reported in a few diseases (11, 12) though they have not necessarily been identified as a causative agent and to date compelling evidence for HERV-K protein involvement in cancer is lacking. In immunohistochemical studies performed in this lab on human normal and tumor tissue arrays using our anti-HERV-K Env surface (SU) monoclonal antibodies, levels of expression of HERV-K in tumor tissue correlate strongly to progression of disease state in cancer patients (13).

1.1.2 Genomic and Structural features of HERV-K

As endogenous retroviruses are genetic remnants of once-active pathogens that were once able to infect and integrate their genetic material into host cells, their genome is highly similar to modern exogenous retroviruses such as HIV. In an intact, mature betaretroviral virion, the genome exists as a double stranded (+) sense linear RNA polymer approaching 10 kb in size and forms the viral ribonucleoprotein complex when in association with the nucleocapsid. Viral protein coding regions are flanked by long tandem repeats (LTRs) which contain regulatory regions to control expression of viral genes including *gag*, *pol*, and *env*. The Env protein is composed of SU and TM (transmembrane) domains and along with Gag and Pol, the integrated proviral genome of HERV-K coding for these proteins is largely intact as depicted in Figure 1. A mature betaretrovirus appears as an approximately 100 nm spherical particle under the electron microscope and bears structural similarity to the particle depicted in Figure 2.

As a retrovirus outside of the host, HERV-K would rely on RT for successful integration into the host genome subsequent to infection. This enzyme, encoded by the *pol* gene, allows the virus to convert its RNA-based genome into DNA via reverse transcription. If these infection and stable integration events occur in germ cells, the viral sequences will be transmitted horizontally from parent to progeny; it is commonly held that this is the mechanism by which HERV retroviral elements exist as they do today in the human genome. HERV-K is of great interest among all the retroviral elements found in the human genome because of its relatively recent integration, transcriptional activity, and existence of open reading frames at various loci across the human genome for many

of its proteins. Functional envelope and reverse transcriptase proteins of a retrovirus are prerequisites for virulence; we therefore focused on their detection.

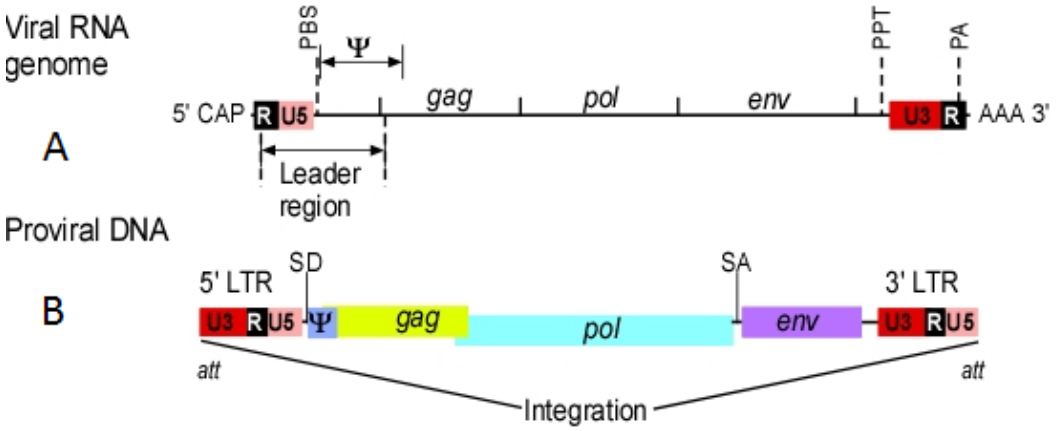

Figure 1a,b (A) Genomic organization of an example of oncoretrovirus proviral DNA, and (B) retroviral RNA transcripts. The full-length transcript serves as the RNA genome and as a messenger RNA for Gag and Gag/Pol polyproteins. The Env is translated from the spliced transcript. Reprinted from (14) under open access policy of International Archives of Medicine (BioMed Central).

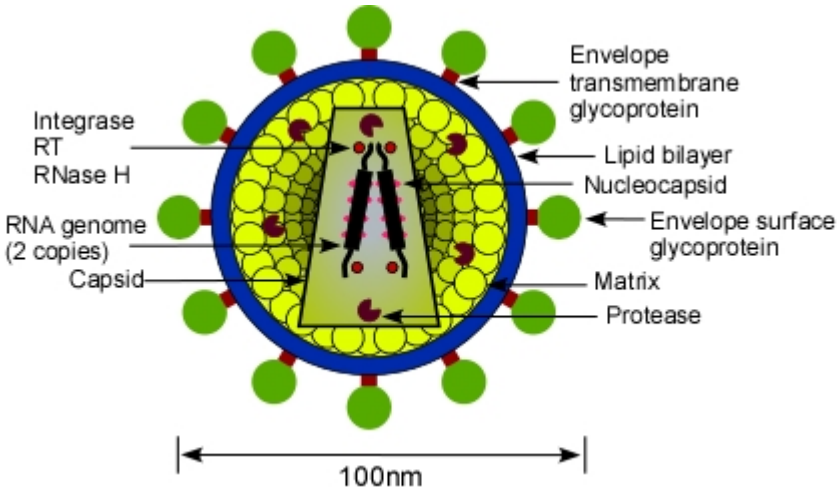

Figure 2 Schematic diagram of retroviral virion structure. Reprinted from (14) under open access policy of International Archives of Medicine (BioMed Central).

1.1.3 HERV Classification and taxonomy

A phylogenetic tree has been created for human endogenous retroviruses as shown in Figure 3. HERVs have been divided into three classes by comparing their homology to relatives from Retroviridae. HERV class I bears the most resemblance to modern gammaretroviruses and includes HERV-H, -W and –FRD. Class III HERVs, showing similarity to spuma-like viruses, include HERV-L and HERV-S. HERV-K, the focus of this study, is a member of class II and aligns most closely with modern betaretroviruses such as MMTV. HERVs are commonly named for the host tRNA used to prime reverse transcription and accordingly HERV-K utilizes lysine tRNA for this purpose. Sequencing of the primer binding site region of the HERV LTR will tell which tRNA is used; this naming convention becomes inadequate when two HERVs are found to use the same tRNA (16).

Most HERVs appear to have integrated long ago, as they are present in the genomes of Old World primates such as macaques and baboons as well as those of New World primates. This suggests infection by the oldest pathogenic progenitor of HERV at least 40 million years ago when these primates diverged. Determinations of when each HERV infiltrated the human genome rely on comparison of LTR regions both in the same HERV and between different classes of HERV. This information, along with estimates of LTR mutation rate over time, can be used to determine the timeframe of infection for a given HERV.

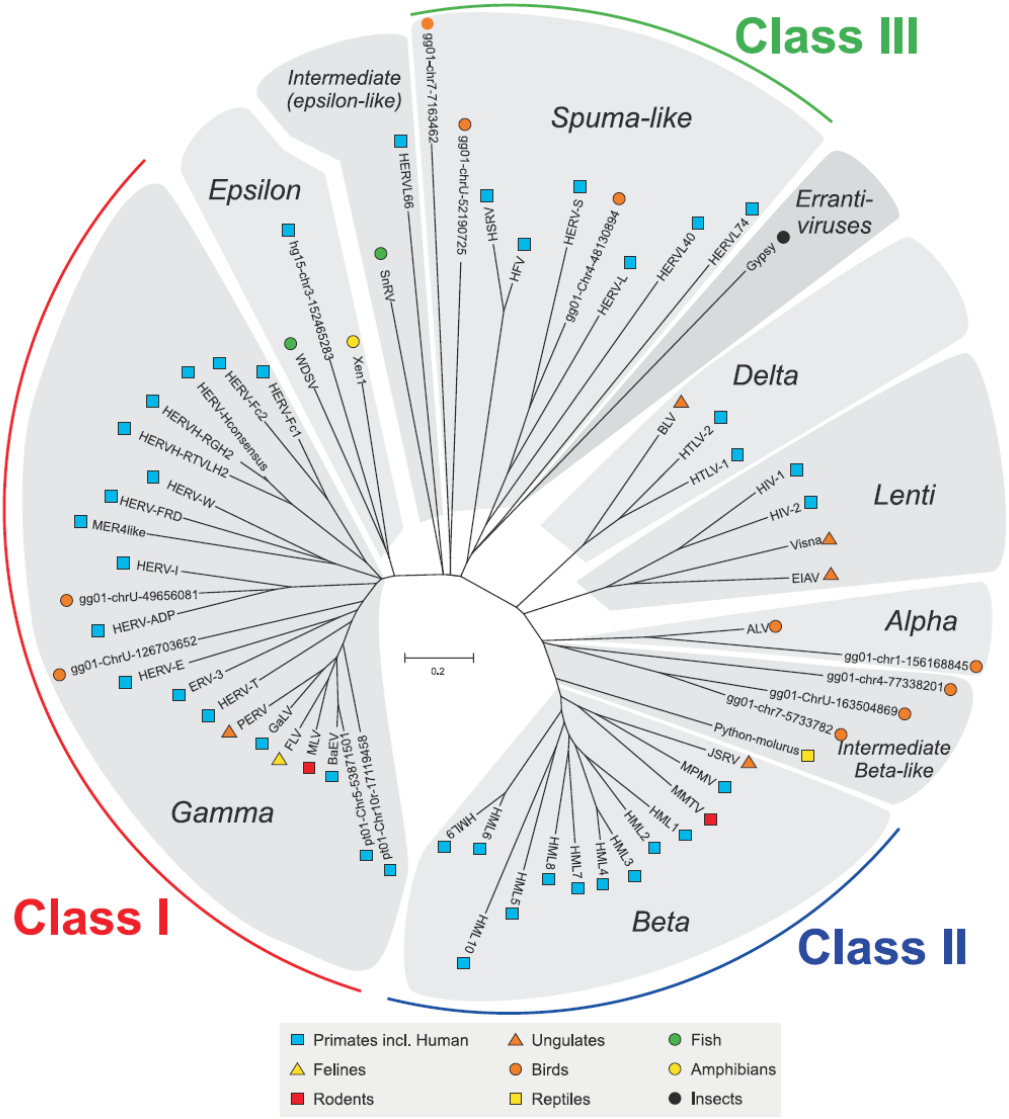

Figure 3 Phylogenetic tree of endogenous and exogenous retroviruses. Representative unrooted neighbor joining dendrogram based on retroviral Pol sequences. HERV-K is denoted as HML2 with class II betaretroviruses.
Reprinted from (15) under open access policy of Retrovirology (BioMed Central).

1.2 Human Cancer and HERV-K

1.2.1 Impact of cancer on women

The World Health Organization has identified cancer as the leading cause of death worldwide (17). Cancer is destined to kill millions of people a year until a cost-effective treatment with broad-reaching efficacy is discovered. Several modern niche drugs exist which can be incredibly effective in specific subsets of the patient population, though they typically lack the diverse applicability of traditional, front-line disease management strategies including surgery, radiotherapy, and chemotherapy. Worldwide, breast cancer has the highest incidence of any cancer in either men or women. The rate of incidence for ovarian cancer is significantly lower (84%) than breast cancer, however the rate of mortality is almost double that of breast cancer (17). The prevalence and the low long-term survivability of these diseases, the impact on overall quality of life for those who endure treatment, the great financial and personal stress on both patients and their families, compounded by the issue of higher overall risk for developing secondary tumors and other diseases if the patient survives treatment, warrants identifying meaningful diagnostic screening tools for early detection and safe, efficacious therapies after diagnosis. Science and medicine must dedicate as many resources as possible to eradicate these devastating diseases. The current state of screening, treatment, and long-term management of cancer stands on the back of decades of hard-learned lessons about the complexity of cancer as a disease that is as unique as the patient that presents with it. Modern molecular diagnostics have enabled the development of personalized treatment regimens for cancer patients based on

characteristics unique to a patient's individual disease. As with all cancers, the best chance for tumor cure in breast and ovarian cancer lies in early detection.

1.2.2 HERV-K in breast and ovarian cancer

HERV-K *env* SU mRNA and HERV-K Env protein has been reported to be overexpressed in breast and ovarian cancer but absent in normal tissues (13, 18, 19). HERV-K viral-like particles were also reported in T47D, a commercially available (20), as well as the blood of lymphoma and breast cancer patients but not in normal samples (21). Taken together, these reports suggest the HERV-K virus or viral-like particles may be shed from HERV-K^+ malignancies and their presence can be used as to screen for cancer.

1.2.3 Targeting of tumor markers using antibody-based drugs

There exists among the cancer research community a great interest in identifying novel tumor-associated and ideally tumor-specific antigens that can be exploited to fulfill both diagnostic and therapeutic healthcare needs in oncology. Identification and characterization of novel antigens that are differentially expressed between tumor and normal tissues is a primary focus of a large contingent of both public and private research efforts. Clearly, the ultimate goal of this enormous outpouring of effort and funding is the discovery and validation of marketable drugs for use in the clinic against a given disease state. If an antigen can be found stably overexpressed in abundance in neoplastic tissues relative to normal examples, a new potential diagnostic and possibly therapeutic target will have been found. A limited number of such antigens have been well-described to date; examples include vascular endothelial growth factor A (VEGF-A), oncofetal proteins carcinoembryonic antigen (CEA) and alpha-fetoprotein (AFP) in

bowel and germ cell tumors, respectively, mucin-1 (MUC-1), and Her2/neu in breast cancer. Many potential tumor-associated targets present unique pharmacological challenges including low abundance, high degrees of target sequence variation, and poor immunogenicity. As a result, development of therapeutic compounds and dosing strategies thereof showing broad-ranging activity as well as minimized off-target effects has been a perplexing challenge. Humanized antibodies have been developed against the above targets (Bevacizumab (VEGF), Clivatuzumab tetraxetan (Muc1), Labetuzumab (CEA), Tacatuzumab tetraxetan (AFP), and Trastuzumab and Pertuzumab (Her2)) with the hopes of utilizing these molecules in the clinic. As evidenced by the development of tetraxetan conjugates above, as well as other immunoconjugates, there is an interest in modifying antibodies to enable them to deliver active agents directly to tumors .

Examples of antibody-based immunoconjugate drugs that have shown enough promise to enter clinical trials include those that bear proteinaceous toxins (22, 23), isotopes (24), chemotherapy drugs (25), and prodrugs (26). Along with current studies using existing chimeric or humanized antibodies recognizing the well-defined tumor markers mentioned above, new targets have emerged as our understanding of tumor cells induction, growth, and metastasis grows. Through identification and characterization of novel tumor-associated antigens such as HERV-K Env, we hope to increase the availability of safe and efficacious reinforcements in the supply of current clinical armaments.

1.3 Hypothesis and specific aims

Reports of expression of human endogenous retroviral mRNA and protein in tissues isolated from cancer patients and the lack of these viral markers in normal tissues (13, 18) prompted us to attempt to identify HERV-K particles shed from HERV-K^+ tumors into the blood circulation of cancer patients with the ultimate goal of identifying mature, infectious HERV-K virions. Based on these previous findings, **we hypothesize that HERV-K viral proteins RT and Env SU are tumor-associated proteins, the presence of which can be exploited for diagnostic and therapeutic purposes.** We tested this hypothesis by carrying out the following two specific aims.

Specific aim 1. To determine the prevalence of reverse transcriptase enzyme activity in cancer patient plasma samples compared to normal donors as a potential diagnostic marker.

Specific aim 2. To determine the potential of antibodies recognizing HERV-K Env SU for use as diagnostic and/ or therapeutic agents.

Chapter 2 Materials and Methods

2.1 Cell lines, clinical samples, and animals

Human breast cancer cell lines T47D, ZR-75-1, and SK-BR-3 were purchased from ATCC (Rockville, MD) and cultured as per ATCC recommendations. The human pancreatic cancer cell line Panc-2 was also obtained from ATCC and cultured as per ATCC recommendations. The breast adenocarcinoma cell line MDA-MB-231 as a kind gift from Dr. Michael Rosenblum (M. D. Anderson Cancer Center, Houston, TX) and was cultured in RPMI-1640 media containing 10% FBS, 100 U/ml penicillin, and 100 μg/ml streptomycin. The breast adenocarcinoma cell line MCF-7 was a kind gift from Dr. Melinda Hollingshead (Developmental Therapeutics Program, Division of Cancer Treatment and Diagnosis, NCI) and was cultured in RPMI-1640 media containing 10% FBS, 100 U/ml penicillin, and 100 μg/ml streptomycin. The fibrocystic breast disease-derived cell line MCF-10A was a kind gift from Dr. Robert Pauley (Karmanos Cancer Institute, Detroit, MI) and was cultured in Dulbecco's Modified Eagle Medium : Ham's Nutrient Mixture F12 (DMEM:F12) medium containing 5% horse serum, 100 U/ml penicillin, 100 μg/ml streptomycin, 10 μg/ml insulin, and 20 ng/ml epidermal growth factor. MCF-10AT, the H-Ras-transformed variant of MCF-10A, was a generous gift from Dr. Fred Miller (Wayne State University, Detroit, MI) and was cultured in the same media formulation as MCF-10A detailed above. Murine hybridoma lines 6h5 and 6e11, producing monoclonal antibodies against HERV-K Env SU, were produced under contract with Auburn University Hybridoma Facility, Auburn AL.

With informed consent, patient plasma, sera, and tissues were obtained from human patients through Institutional Review Board (IRB)-approved protocols in place at

M.D. Anderson Cancer Center, Houston, TX. Gender-matched healthy donor buffy coats were purchased from Gulf Coast Regional Blood Center, Houston, TX.

6-8 week old female Balb/c (National Cancer Institute, Frederick, MA) mice were used for the generation of ascites fluid from which the monoclonal antibodies 6h5 and 6e11 were purified. 8 week old NOD-SCID gamma mice, a kind gift from Dr. Dean Tang (M. D. Anderson Cancer Center, Smithville TX), were used for MDA-MB-231 and Panc-2 xenograft studies.

2.2 Monoclonal antibody production

Production of ascites containing monoclonal antibodies were carried out under an IACUC-approved ACUF. Hybridoma lines were maintained in suspension culture in RPMI-1640 including 1mM oxaloacetate, 0.45 mM pyruvate, 0.2 U/ml insulin, 100 μM hypoxanthine, 16 μM thymidine, and 10% FBS in T75 flasks. The cells were treated with 30 μg/ml mitomycin C for 30 minutes and washed twice in PBS immediately prior to injection.

20 Balb/c mice were primed using 0.5 ml of pristane administered to the peritoneal cavity 2 weeks before $5x10^6$ mitomycin c-treated hybridoma cells were injected ip. At the onset of edema, ascites was drained from the peritoneal cavity by 18 gauge needle; this was repeated twice as needed over the course of a few weeks to relieve accumulated fluid. Animals were sacrificed by CO_2 asphyxiation and subsequent cervical dislocation upon completion of three ip taps. Harvested ascites was centrifuged at 500 xg for 5 minutes to remove cells and coagulates. Ascites generated from the same hybridoma were collected, pooled, and thoroughly admixed. 10 ml aliquots of this clarified supernatant were frozen at -80° C for future purification.

Antibody was purified by thawing a 10 ml aliquot of ascites fluid on ice then diluting it 1:1 with cold PBS. This diluted ascites was centrifuged at 500 xg at 4° C to remove cryoprecipitates; the supernatant was retained and an equal volume of saturated ammonium sulfate was added drop-wise while mixing. This preparation was incubated overnight at 4° C with continuous mixing. The next day the sample was centrifuged at 10,000 xg for 30 minutes at 4° C to pellet precipitated proteins. This pellet was resuspended in PBS and the ammonium sulfate precipitation process was repeated once more as described above. The final pellet of precipitated protein was resuspended in PBS and clarified with a 0.45 μ CA filter. This clarified, double salt-cut ascites was purified on an ÄKTA FPLC using a Protein G HP affinity resin column (GE Healthcare); antibody was eluted in 0.1 M glycine pH 2.5 directly into fraction collection tubes pre-loaded with one-tenth volume 1 M Tris base pH 9 to immediately neutralize the low pH of the elution buffer. Protein-containing fractions, as determined by on-line 280 nm UV absorbance monitoring, were pooled and dialyzed overnight against PBS at 4° C using a Slide-a-Lyzer 3 kDa MWCO dialysis cassette (Pierce).

Antibody preparations intended for cell dosing were further purified using Detoxi-Gel polymixin B affinity resin (Pierce) to remove bacterial lipopolysaccharides (endotoxin). Total protein concentration was determined by UV spectrophotometry at 280 nm. All antibodies were sterilized using 0.2 μ SFCA filtration and aliquots of purified antibody stored in -80° C for future use.

2.3 Antibody isotype determination

To determine the isotype of 6h5 and 6e11 monoclonal antibodies, 100 µl of confluent hybridoma culture media was tested using a mouse antibody isotyping test strip kit (AbD SeroTec, Raleigh, NC) per the manufacturer's instructions.

2.4 Antibody conjugation to AuNP

The isoelectric point of 6h5 was determined by isoelectric focusing. One mg of 6h5 was dialyzed against distilled water pH 7.4 overnight at 4º C. 500 µg of dialyzed 6h5 was incubated with 50 ml of 5 nm or 30 nm colloidal gold (Ted Pella, Redding, CA) at pH 7.4 with gentle agitation for 15 minutes at room temperature. The conjugate was loaded into a 30 ml dialysis cassette (Slide-A-Lyzer; Pierce, Rockford, IL), wrapped in cheesecloth, and left buried in drying resin (Silica gel Rubin; Sigma-Aldrich) overnight. This pre-concentration process was repeated until the sample volume was approximately 3 ml. A 30-ml column of Sephacryl S-500-HR (GE Healthcare) was prepared and unincorporated label was removed by size-exclusion chromatography using ÄKTA FPLC. Fractions containing mAb-AuNP conjugate as determined by online A_{280} monitoring were pooled, stabilized with 0.1% polyethylene glycol 1000, and concentrated using 3kDa molecular weight cut off centrifugal concentrators (Amicon Ultra; Millipore, Billerica, MA).

2.5 HERV-K^+ xenograft labeling with 6h5-AuNP conjugate

Murine xenograft models were carried out under an IACUC-approved ACUF. 8 week old NOD-SCID gamma mice were inoculated sc in the right flank with $5x10^6$ MDA-MB-231 or Panc-2 tumor cells. Once tumors reached 1cubic centimeter, 25µg (by protein) of 6h5-AuNP conjugate (5 nm AuNP for MDA-MB-231 and 30 nm AuNP for

Panc-2) were administered iv via the caudal vein. 24 hours after dosing, the mice were euthanized and tumors were excised. The tumor tissue was minced and fixed in 2% paraformaldehyde and 2.5% glutaraldehyde in 0.1 M sodium cacodylate buffer pH 7.4 overnight. The tissue was counterstained in 2% aqueous uranyl acetate (UA) for 1 hour, washed, and post-fixed in OsO_4-KFeCN for 2 hours in the dark. The tissue was then dehydrated through increasing concentrations of ethanol, then with acetone previously dehydrated using a water-sequestering molecular sieve (type 3A, Sigma). The sample was then infiltrated with Spurr's low viscosity resin (Structure Probe Incorporated, West Chester, PA) and cast into blocks by heat polymerization, which was accomplished by baking for 2 days at 80° C. Thin sections were cut with an Ultra 35 diamond knife (Diatome, Hatfield, PA)-equipped Ultracut UCT (Leica) and captured on pre-cleaned bare copper grids. Section were imaged on a Spirit TEM (Tecnai, Hillsboro, OR) operating at 80 kv.

2.6 Synthetic HERV-K Env SU antigen production

An open reading frame for HERV-K Env SU was cloned into the bacterial expression vector pGEX-6p1and transformed into chemically competent *E. coli* BL-21 (DE3). Subclones were screened for soluble fusion protein expression; clone K10g was chosen, which expresses a full-length HERV-K Env SU bearing an N-terminal GST affinity tag.

The clone K10g was streaked onto a fresh LB-agar plate containing 50 μg/ml ampicillin and incubated overnight at 37° C. A single colony was picked and used to inoculate a 3 ml starter culture of K10g in Super Broth (35g tryptone, 20g yeast extract, 5g NaCl in dH2O) containing 50 μg/ml ampicillin overnight at 37° C with 250 rpm

agitation. This starter culture was used to inoculate 1 L of Super Broth including 1 mM $MgSO_4$ and 50 μg/ml ampicillin in baffled flasks with 250 rpm shaking. After reaching OD_{600} of 1.0 (where the maximum OD_{600} of the culture system is ~1.5), the culture was induced with 1 mM IPTG at 18° C overnight with continued shaking at 250 rpm. The culture was harvested in a Sorvall Evolution RC superspeed centrifuge equipped with a SLA-3000 rotor at 6,000 xg for 15 minutes.

Bacterial culture pellets were resuspended in 3 ml per gram of wet pellet weight of PBS + 1 mM EDTA + 1 mg/ml lysozyme and incubated on ice for 1 hour. The digested pellet was sonicated 4 times total, 25 ml at a time on ice using four 10 second cycles at ~100 watts power output. Foaming was avoided and the sample was allowed to cool for 1 minute between cycles. Lysis was confirmed by drastic reduction in viscosity and partial clarification of the sonicated sample. This material was centrifuged for 30 minutes at 50,000 xg at 4° C and further clarified with a 0.45 μ SFCA filter.

The clarified lysate was applied to a glutathione resin column connected to an ÄKTA FPLC. Samples were eluted using freshly-prepared 10 mM reduced glutathione in 50 mM Tris base pH 8. Protein-containing fractions, as determined by on-line A_{280} monitoring, were pooled and dialyzed overnight against a 400-fold excess of PBS with constant stirring at 4˚ C using a Slide-a-Lyzer 3kDa MWCO dialysis cassette (Pierce). Aliquots of all purified materials were stored in -80° C for future use.

2.7 Antibody kinetic and concentration analysis

Biacore technology exploits the phenomenon of SPR to analyze biomolecular interactions. All Biacore experiments were carried out at 25° C and used HBS-EP running buffer. Calibration-free concentration analysis (CFCA) was performed on the

Biacore X100 biosensor platform which detects binding of the antibody in solution flowing over a surface of immobilized K10g antigen. K10g immobilization conditions were scouted by injecting 30 nM K10g in 10 mM sodium acetate at pH 4, 4.5, 5, and 7 over a naïve CM5 chip surface. Regeneration scouting was performed using 300 nM 6h5 to test four different regeneration conditions. Five cycles of binding and regeneration were carried out using 30 second injections of either 2 M $MgCl_2$ in 5 mM glycine pH 2, 5 M NaCl pH 7, 100% ethylene glycol, or 10 mM NaOH pH 12 and both baseline and response data was plotted.

For CFCA, a high degree of ligand density immobilization is required. Two flow cells of a CM5 chip were activated using 50 mM EDC + 200 mM NHS in water for 2 minutes. The test flow cell had ~7500 RU of K10g immobilized on the surface; once adequate ligand was bound, unreacted immobilization sites were quenched with 1 M ethanolamine pH 8.5 for 4 minutes. On the same chip a blank control flow cell was prepared where no ligand was immobilized (activation and quenching only). Dilutions of analyte were prepared at 1:1, 1:10, 1:100, and 1:1000 to span a wide range of concentrations. These dilutions were simultaneously injected in duplicate across both the K10g ligand and blank flow cell surfaces at 10 µl/min and 100 µl/min to determine the effect of flow rate on mass transport limitation. Our molecular diffusion constant (D) was $5e^{-11}$ m^2/sec for 6h5 and 6e11 in water at 20˚C. The resulting SPR sensorgrams were then analyzed using Biacore X100 Evaluation software to determine the active analyte concentration. These concentrations as determined by CFCA were used in subsequent kinetic analysis as well as other experiments. Fitting statistics are a crucial part of interpreting data generated by SPR; for CFCA experiments a χ^2 value is

calculated by the evaluation software to indicate "goodness-of-fit" to ideal binding equations. Ideally, χ^2 values for quality data should be less than 5% of the R_{max} of the slower flow rate. Another metric generated by the evaluation software is a QC ratio, which ideally should be close to 0.2 for confident results.

In order to obtain kinetic binding constants for 6e11 and 6h5 against the recombinant cognate antigen K10g, we also employed the Biacore X100 platform. A CM5 chip was docked to the Biacore X100 instrument and 30 μl/min flow was initiated. Two flow cells of a CM5 sensor chip were activated using 50 mM EDC + 200 mM NHS in water for 2 minutes. Approximately 200 RU of K10g in 10 mM sodium acetate pH 4.5 was immobilized onto the test flow cell. Once 200 RU of K10g ligand was accumulated on flow cell two, both flow cells were quenched by injecting 1 M ethanolamine pH 8.5 over both surfaces for 4 minutes. The chip was primed 5 times before the binding experiment was carried out. A series of duplicate antibody concentrations of 0, 3, 6, 12, 24, and 48 nM were then injected simultaneously over both the test and control flow cells.

SPR sensorgrams from ligand-immobilized flow cells was normalized by subtracting the signal from the blank flow cell; resulting data generated from these kinetic experiments were fitted to a 1:1 Langmuir thermodynamic binding model in the Biacore X100 evaluation software. The Evaluation software reported thermodynamic constants as well as statistical fitting parameters from these fitted curves; χ^2 values at or less than 1% of R_{max} are considered ideal and indicate a good fit to the chosen binding model.

2.8 Isopycnic (density gradient) fractionation

To identify HERV-K viral components in human plasma, heparinated blood was overlaid on Histopaque 1077 (Sigma, St. Louis, MO) density gradient media and centrifuged at 400 xg for 30 minutes at room temperature. The plasma layer was retrieved and 10 ml were used for isopynic separation of viral particles. Isolation of viral particles was carried out using OptiPrep® iodixanol (AxisShield, Norton, MA) density gradient medium by diluting 10 ml of plasma into 28 ml total volume with PBS. This sample was loaded into a polyallomer ultracentrifuge tube and 4 ml of a 50% solution of iodixanol in PBS was underlaid. This sample was centrifuged at 111,800 xg (average) for 90 minutes in an AH629 swinging bucket rotor in a Sorvall UltraPro 80 ultrarcentrifuge. After this pre-concentration step, the top 22 ml of media was discarded and the remaining sample was mixed with the underlying iodixanol cushion to give a final sample concentration of approximately 20% iodixanol. The samples were the loaded into crimp-top polyallomer tubes at centrifuged for 5 hours at 314,543 xg (average) in a T865.1 fixed-angle rotor. Samples were carefully removed from the rotor to avoid disturbing the gradient and each tube was punctured at the top and bottom. 200 µl fractions were drained from the bottom of the tube in order of decreasing density and collected into sample tubes. The remainder of the sample in the gradient was collected into 2 ml fractions also in order of decreasing density and archived. Viral particles isolated by isopycnic fractionation were kept at -20° C for further analysis.

Isopycnic fractionation of viral particles from conditioned cell culture media from MCF-7 was carried out in the same way as plasma described above, only 28 ml of

undiluted media was used in lieu of diluted plasma and 6 fraction preparations were pooled and analyzed.

2.9 Patient tissue viral particle isolation

100 mg of snap-frozen patient tissue was homogenized using a conical mortar and pestle in 1 ml of RPMI-1640 + 10% FBS. This triturate was then passed through a 0.45 μ SFCA filter, divided into aliquots, and stored frozen at –80° C for future analysis. These samples were used only in RT-PCR experiments.

2.10 Reverse transcriptase assay

Patient plasma density gradient fractions were thawed and mixed thoroughly. 50 μL was removed and dissociated with 10 mM Tris base pH 8.0 + 0.2 mM DTT + 0.2% Igepal CA-630 with constant agitation at room temp for 1 hour. Dissociated viral particles were assayed for RT activity using EnzChek RT Assay (Invitrogen, Carlsbad, CA) as per manufacturer's instructions. This assay uses RT enzyme from the sample to carry out reverse transcription on a pre-annealed poly (A) primer and oligo dT template. The resulting RNA:DNA heteroduplexes are stained with PicoGreen and the plate is read in fluorescence mode with a Victor V plate reader (Perkin Elmer, Waltham, MA).

2.11 RT-PCR

Viral RNA was purified from 50 μl of each tested gradient fraction using the MinElute Viral RNA purification kit (Qiagen). vRNA was eluted in 50 μl of buffer AVE; 5 μl of this eluate was used for RT-PCR using K10 (type 1) and K22 (type 2) primers. Total RNA from the HERV-K^+ malignant breast adenocarcinoma cell line SK-BR-3 (ATCC, Manassas, VA) was used for K10 and K22 positive control. Template-free negative controls were included as well to test for contamination of reaction

components. An aliquot of each viral RNA was also treated with 0.1 mg/ml RNase A for 1 hour at 37˚ C and setup as a parallel reaction with K10 primers to determine the contribution of genomic DNA contamination to the PCR result. Subsequent RT-PCR was carried out using the OneStep RT-PCR kit (Qiagen) to amplify Type 1 and Type 2 HERV-K Env SU vRNAs using K10 sense (5'-AGAAAAGGGCCTCCACGGAGATG-3'), K22 sense (5'-GTATGCTGCTTGCAGCCTTGATGAT-3'), and K10 antisense (3'-ACTGCAATTAAAGTAAAAATGAA-5') primers. Type 1 and type 2 HERV-K amplicons are both generated using the same antisense primer. 5 µl of each vRNA was used as the template in each reaction with a final reaction volume of 18 µl. Hot start PCR was carried out on a DNA Engine (PTC-200, Bio-Rad) thermocycler using the following program: 50° C for 30 minutes (reverse transcription reaction), 95° C for 15 minutes (required for activation of HotStart Taq polymerase), then 35 cycles of 30 seconds at 94° C, 30 seconds at 55° C, and 1 minute at 72° C. A final extension for 10 minutes at 72° C completed the RT-PCR. RT-PCR reactions were resolved by 1% agarose gel electrophoresis in TAE (40 mM Tris-acetate + 1mM EDTA) buffer; once the reaction was complete, 6x gel loading buffer was added directly to the reaction, the entire sample was loaded into the gel and resolved by electrophoresis for 75 Vhr. Gels were stained in TAE buffer containing 0.5 µg/ml ethidium bromide for 1 hour with gentle agitation and imaged on a gel documentation system using UVB transillumination (Gel Doc 1000, Bio-Rad). Amplicons of interest were excised from the gel under brief UV transillumination and purified from the gel slice using QIAquick Gel Extraction kit (Qiagen), with elution in 10 mM Tris-Cl pH 8.5. Concentration was determined by NanoDrop (ND-1000, NanoDrop Technologies Wilmington, DE) and submitted for

unidirectional sequencing to the Science Park Research Division – Center for Research on Environmental Disease SPRD-CRED Molecular Biology Core in the Molecular Carcinogenesis Department at MD Anderson Cancer Center using the 5' PCR primer. Sequencing results were aligned to known HERV-K sequences in PubMed using NCBI's BLAST.

2.12 1-D SDS-PAGE and Western Blot

For K10g, a 10% acrylamide denaturing SDS-PAGE was carried out. 10 μg of purified protein was heated in reducing Laemmli sample buffer at 95˚ C for 10 minutes before loading onto the gel. For 6h5 and 6e11, 10 μg of purified antibody were heated in non-reducing Laemmli sample buffer at 95° C for 5 minutes before loading onto a 4% SDS-PAGE gel. A pre-stained molecular weight reference marker was included on all SDS-PAGE experiments. Samples were resolved by electrophoresis in Laemmli running buffer for 100 Vhr. At this point gels bound for coomassie stain were removed and fixed in destain solution (10% acetic acid, 40% dH2O, and 50% methanol) for 30 minutes. The gels were then stained for 10 minutes in a coomassie R250 solution (50% methanol, 40% dH2O, 10% acetic acid + 0.25% coomassie R250) that was preheated to 65˚ C and subsequently bathed in destain solution until protein bands became clearly visible and the level of background stain was acceptable. These coomassie-stained gels were dried onto filter paper using a SGD 4050 gel dryer (Thermo-Savant, Waltham MA) at 65° C for 3 hours. Samples bound for western blotting were removed, sandwiched in the transfer cassette of the Mini-Protean 2 wet blotting apparatus (Bio-Rad) between filter paper and adjacent a piece of 0.2 μ PVDF membrane prewetted with pure methanol and equilibrated in transfer buffer. The transfer was carried out at 60 mA overnight at 4˚ C.

The next day the membranes were removed, blocked in PBS + 0.2% Tween 20 + 3% BSA for 1 hour at room temp with gentle agitation, and probed with the indicated antibodies.

For western blot of total cell lysates, cells were cultured to 95% confluence in the media formulation recommended by ATCC. Cells were washed in PBS, resuspended in 1% CHAPS + protease inhibitor cocktail (Roche, Indianapolis, IN) and frozen overnight at -80° C. Total protein concentration of clarified lysates was determined by Bradford assay and 50 μg of lysate were boiled in Laemmli sample buffer and resolved by 10% SDS-PAGE along with a lane of Kaleidoscope Precision Plus ladder (BioRad, Hercules, CA). PVDF was pre-wetted in methanol and equilibrated in Laemmli transfer buffer; samples separated on the SDS-PAGE gel were wet-transferred onto this conditioned PVDF membrane overnight at 60 mA at 4° C. The next day membranes were blocked with 3% BSA in TBS+0.2% tween 20 for 1 hour at room temp with gentle agitation. 1 μg/ml 6h5 was added for 1 hour in blocking buffer and rinsed thoroughly in TBS-0.2% tween 20. 1 μg/ml anti-mouse IgG-HRP conjugate was added for 1 hour at room temp in blocking buffer and washed thoroughly in wash buffer, followed by TBS only. ECL reagent (Western Lightening Plus, Perkin Elmer) was added to the membrane and exposed for various amounts of time to Biomax light ECL imaging film (Kodak, Rochester, NY). Films were developed using standard developer and fixer chemistry (Merry Xray, San Antonio, TX).

Patient plasma fractions were prepared for western blotting by chloroform:methanol precipitation. To 25 μl of each plasma fraction, 100 μl of methanol was added and the sample was vortexed for 5 seconds. 25 μl of chloroform was then

added and vortexed again. 75 µl of dH2O was then added and vortexed. The sample was then centrifuged at 15,000 xg for 2 minutes and the supernatant discarded. 100 µl of methanol was added to the pellet, vortexed again, and centrifuged at 15,000 xg for 2 minutes. The supernatant was discarded and the remaining solvent was purged from the sample by drying the pellet in a SpeedVac (Thermo-Savant) for 10 minutes. The pellet was dissolved in Laemmli sample buffer modified with 6 M urea, 1% CHAPS, and 50 mM DTT. Samples were resolved by 10% SDS-PAGE, transferred onto PVDF membranes, and blocked with 5% non-fat milk in TBS + 0.2% tween 20 (BLOTTO). The blocked membranes were probed with 10 µg/ml 6e11 for 1 hour at room temperature, washed in TBS + 0.2% tween 20 (TBS-T), and probed with 10 µg/ml anti-mouse IgG-HRP. After thorough washing in TBS-T, the membranes were rinsed in TBS, and ECL reagent (Western Lightening Plus, Perkin Elmer) was added to the membrane and exposed for various amounts of time to Biomax light ECL imaging film (Kodak, Rochester, NY). Films were developed using standard developer and fixer chemistry (Merry Xray, San Antonio, TX).

2.13 Anti-HERV-K Env SU Antibody Internalization Assay

Antibody internalization assays were performed by culturing adherent cells on pre-cleaned #1.5 glass coverslips in 6 well plates to 90-95% confluence. The cells were rinsed with HEPES-buffered saline (20 mM HEPES + 150 mM NaCl pH 7.4) to remove media components. 10 µg/ml 6e11 or isotype-control mIgG2a (R&D Systems, Minneapolis, MN) in binding buffer (HEPES-buffered saline + 3% BSA pH 7.5) on ice for 1 hour in the dark to minimize phototoxicity related to light-induced HEPES degradation. The cells were then rinsed in fresh binding buffer and room-temperature

cell culture media was added back onto the cells. The plates were placed back in the 5% CO_2 incubator for 2 hours at 37° C. After 2 hours of internalization, cells were fixed in 4% paraformaldehyde in PBS pH 7.4 at room temperature overnight. The next day cells were washed in PBS, permeabilized for 20 minutes in 0.2% Triton X100 in PBS with gentle agitation, and quenched with 50 mM NH_4Cl in PBS pH 7.5 for 30 minutes at room temperature. Cells were rinsed with PBS and blocked with 1% BSA in PBS + 0.2% Tween 20 for 1 hour at room temperature. Polyclonal anti-mouse IgG (H+L) (Pierce, Rockford, IL) was labeled with AlexaFluor 488 CASE (Invitrogen) structureas described by the manufacturer. Anti-mouse IgG-AlexaFluor 488 was incubated with cells for 1 hour at room temperature; cells were then counterstained with 100 nM DAPI for 5 minutes and rinsed twice with PBS + 0.2% Tween 20. Stained cells on coverslips were mounted to standard glass slides in 90% glycerol in PBS, set in place with clear fingernail varnish, and allowed to dry before imaging.

The samples were imaged using a Zeiss Meta 510 Confocal Laser Scanning Microscope equipped with a 63x oil immersion objective; the pinhole aperture was set at 1 airy unit for each channel. Images were captured sequentially using 405 nm excitation for DAPI and 488 nm excitation for AlexaFluor 488. Pinhole aperture diameters were 0.6 μ for the 405 nm channel and 0.7 μ for the 488 nm channel. Tile scan images are a montage of 5x5 scan areas. For the scan speeds utilized, the pixel dwell time was approximately 1.5 milliseconds. 8 bit confocal images were acquired with sequential frame switching at 512 x 512 pixel resolution.

2.14 Transmission Electron Microscopy

Select density gradient fractions from patient plasma showing high RT enzyme activity were prepared for imaging by TEM by 1:100 dilution with PBS. 300 mesh carbon-coated nickel grids (Structure Probe Incorporated) which were prepared by glow discharge in air for 1 minute at 50 mA in an EMITech X100 plasma discharge unit. Diluted plasma fractions were adsorbed onto the glow-discharged grids for 5 minutes; excess liquid was wicked away with a piece of clean Whatman #1 paper (Whatman, Piscataway, NJ). 2% aqueous uranyl acetate (Structure Probe Incorporated) was prepared by thorough vortexing of the counterstain and centrifugation at 20,000 xg for 10 minutes to pellet undissolved uranyl acetate. The grids were counterstained by floating them on a droplet of 2% aqueous uranyl acetate for 3 minutes. Excess stain was wicked away with Whatman #1 paper as described above and the grids were imaged on a Tecnai Spirit TEM operating at 80 kv.

2.15 Statistical Analysis

Patient plasma fraction reverse transcriptase assay results were binned into benign and malignant disease categories for ovarian patient samples and into invasive and *in situ* categories for breast patient samples. Pooled plasma fraction reverse transcriptase enzyme activity results were designated as either positive or negative for RT enzyme activity; a patient considered as having a positive response showed reverse transcriptase activity over 700,000 RFU in any pool tested. These results were tabulated by disease status and percent RT positive was calculated. These binned data were then analyzed by t-test to determine statistical significance of differences in RT activity between samples obtained from malignant tumor patient plasma, benign tumor patient

plasma, and normal donor plasma samples. A significant result obtained a p-value of less than 0.05 by t-test.

Chapter 3 Results

3.1 Monoclonal antibody production

In order to characterize the expression of HERV-K Env SU antigen in our samples, we needed a consistent source of monoclonal antibody that could recognize the viral antigen with high sensitivity and specificity. Production of murine monoclonal antibodies by ascites proved to be an effective strategy from both an economic and product quality perspective. When primed with pristane 7-10 days prior to hybridoma introduction, mice bearing $5x10^6$ hybridoma cells ip will begin to form ascites in the abdomen within 2-4 weeks. Our ACUF provides for 3 taps, which occur within 1-2 weeks with the rapid advancement of both liquid and solid portions of the ascites. It is common to retrieve 10 ml of ascites per animal over the course of tapping in a successful production, which yields approximately 1 mg/ml final affinity purified antibody with activity greater than 50% (the best lot of 6e11 achieved 80% activity). After two rounds of salt-cutting and affinity purification using protein G resin on ÄKTA FPLC, we enjoy single bands by non-denaturing SDS-PAGE from the final dialyzed eluate as indicated in Figure 4. When tested using AbD Serotec's murine antibody isotype kit, both 6h5 and 6e11 tested as IgG2a.

3.2 Recombinant HERV-K Env SU-GST production

As attempting to purify HERV-K Env from natural sources would be a laborious and time-consuming effort at best, we elected to produce a recombinant form of this viral antigen for our studies. Yields of soluble antigen improved with the following modifications beyond the generalized GST fusion protocol suggested by GE Healthcare: 1) amending the media with $MgSO_4$, culturing in baffled shaker flasks, and using the

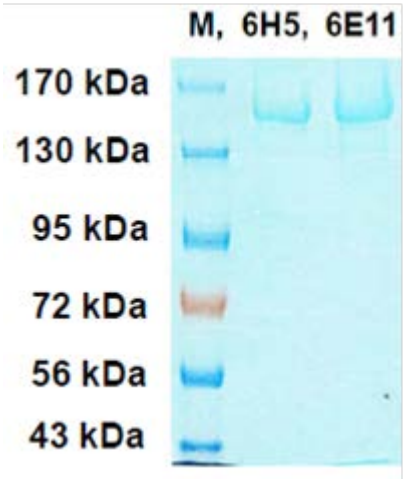

Figure 4 Non-denaturing SDS-PAGE of purified and dialyzed monoclonal antibodies. Reprinted from (27) with permission from Oxford University Press.

richer Super Broth media formulation allowed the culture system to support much higher densities of *E. coli*, allowing induction at a higher culture density, 2) inducing at 18° C overnight instead of the typical 37° C for several hours probably slowed down protein folding kinetics enough to allow for more correctly folded protein per liter of culture and therefore greater soluble yields, and 3) using a combination of lysozyme, EDTA, and sonication (enzymatic, chemical, and mechanical) treatments to maximize lysis of the induced culture after harvest. Figure 5 depicts a coomassie-stained 10% SDS-PAGE and western blot of a representative batch of K10g after affinity purification with glutathione resin on ÄKTA FPLC. The single band at ~67 kDa is evident and the preparation is essentially pure. Four liters of induced shaker flask culture prepared in the manner described can yield several milligrams of soluble K10g, which must be dialyzed into PBS, portioned into aliquots, and stored frozen at or below -20° C to avoid aggregate formation.

3.3 Total cell lysate western blot

Total protein lysates were made from several malignant cancer cell lines as well as MCF-10A and MCF-10AT. 50 μg of each lysate was resolved by SDS-PAGE, transferred to PVDF membrane, and probed for either HERV-K Env SU or ACTB using 6h5 or anti-actin primary and anti-mouse IgG-HRP secondary antibodies. All malignant cell types tested were positive for HERV-K Env SU. MCF-10A, an immortalized cell line derived from a patient with fibrocystic breast disease, was negative for HERV-K Env SU. An H-Ras-transformed variant of MCF-10A, MCF-10AT, showed intermediate expression of HERV-K Env SU, as shown in Figure 6.

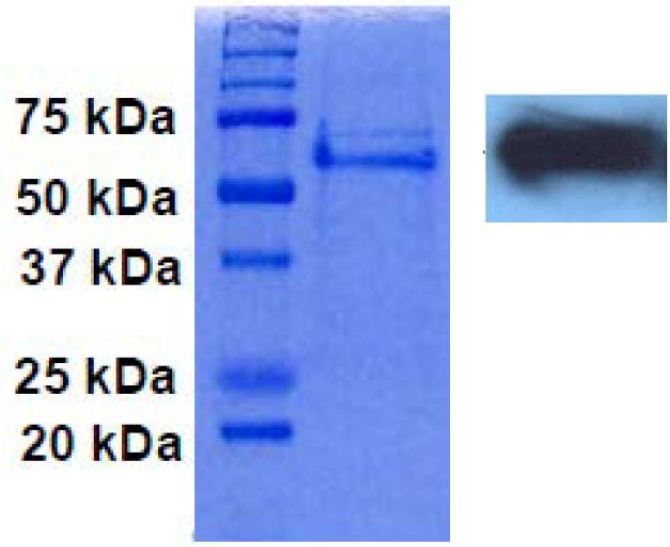

Figure 5 Production of recombinant HERV-K Env SU-GST (K10g). (A) Coomassie-stained SDS-PAGE gel, reprinted from reference (27) with permission from Oxford University Press. (B) Western blot of K10g probed with 6h5.

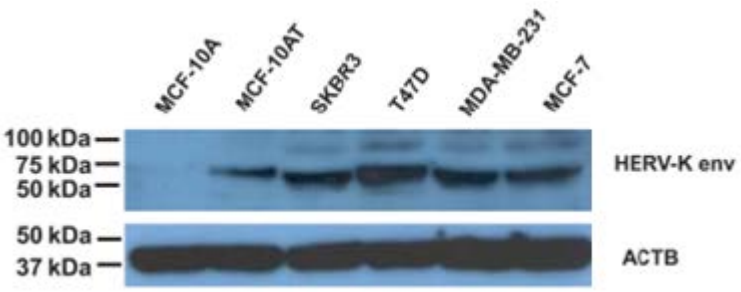

Figure 6 Western blot of HERV-K^+ malignant breast cancer and HERV-K^- breast cell lysates. Reprinted from reference (27) with permission from Oxford University Press.

3.4 Antibody kinetic and concentration analysis

Thermodynamic affinity (K_D) as well as other kinetic binding constants were determined for each monoclonal antibody recognizing K10g using surface plasmon resonance on the Biacore X100 platform. We chose to use CM5 sensor chips, as this chip format is both the most flexible and cost-effective. A low ligand density surface, approximately 200 RU, was prepared for the kinetic analyses and a high ligand density surface, approximately 7500 RU, was prepared for CFCA experiments. Zero ligand density flow cells, which were activated with EDC + NHS then directly quenched with ethanolamine, were also created as control surfaces to determine levels of non-specific interaction and bulk solvent contribution for data normalization purposes during curve fitting and evaluation in the Biacore X100 evaluation software.

CFCA results varied on a per lot basis and representative lots of 6h5 and 6e11 are shown in Figure 7a and b. The K_D values for 6h5 and 6e11 were 1.46 nM and 1.87 nM, respectively, and normalized sensorgrams along with fitted curves are shown in Figure 7c and d. These affinities are optimal for murine monoclonal antibodies, near the limit expected for this type of molecule, and so fulfill the sensitivity requirement for robust diagnostic agents. Lack of significant binding of either antibody to the ligand-free control flow cell addresses and mitigates specificity concerns. Statistical analyses of the kinetic evaluations generated by the Biacore X100 evaluation software are presented in Table 1.

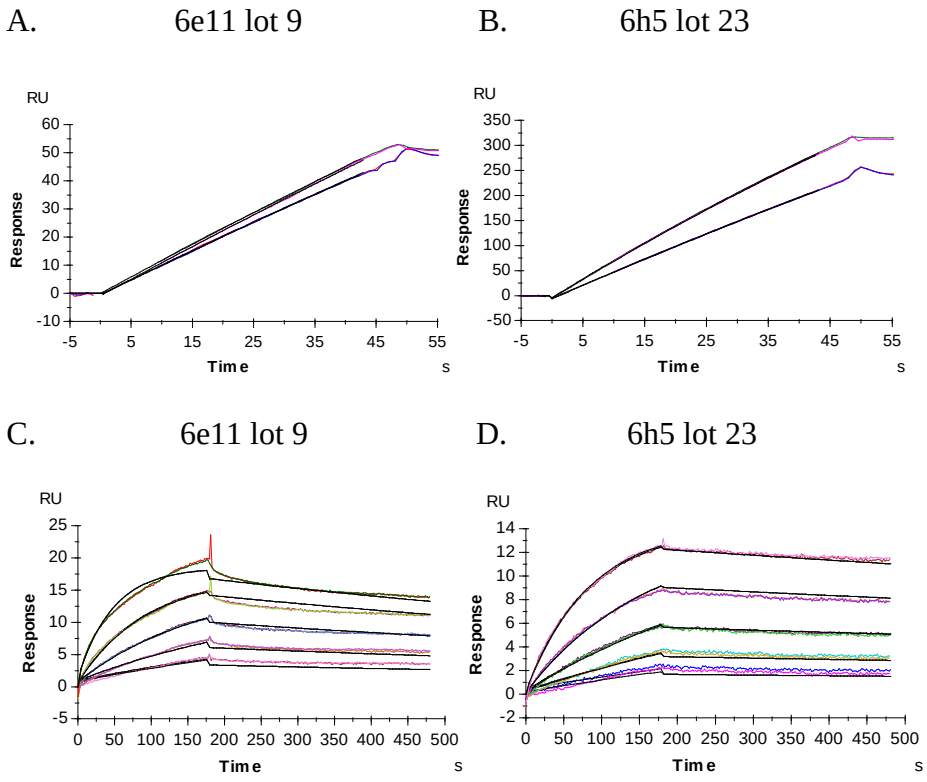

Figure 7a-d – Anti-HERV-K Env SU antibody CFCA (A,B) and kinetic (C,D) SPR sensorgrams. Black lines indicate fitting curves generated by Biacore X100 evaluation software.

CFCA					
	Antibody	**Active Concentration (M)**	**QC ratio**	**Chi² (RU²)**	
	6h5	**9.50E-06**	**0.299**	**0.14**	
	6e11	**5.10E-07**	**0.099**	**0.045**	
Kinetics					
Antibody	**Ka (M-1 s-1)**	**Kd (s-1)**	**KD (M)**	**Chi² (RU²)**	**U-value**
6h5	**2.43E+05**	**3.54E-04**	**1.46E-09**	**0.073**	**5**
6e11	**4.18E+05**	**7.82E-04**	**1.87E-09**	**0.297**	**3**

Table 1 – Anti-HERV-K Env SU antibody CFCA results and kinetic constants with fitting statistics generated by Biacore X100 evaluation software.

3.5 Patient plasma gradient fraction analysis

Reverse transcriptase (RT) enzyme activity in a diverse selection of patient plasma and normal donor density gradient fractions was assayed using the EnzChek RT kit (Invitrogen), which uses a non-radioactive reporter and relies on reverse transcriptase from the test sample generating RNA:DNA duplexes using a provided poly (A) RNA template pre-annealed to an oligo dT primer. Dissociated viral particles isolated from plasma fractions provide reverse transcriptase in our assay and the resulting RNA-DNA heteroduplexes formed by RT enzyme activity are stained and measured using a fluorescent dye which is highly specific for duplex nucleic acids. Samples with greater RT enzyme activity correspond to higher concentrations of nucleic acid heteroduplex which give higher relative fluorescence unit (RFU) readings. Each EnzChek RT assay batch included a Moloney Murine Leukemia Virus Reverse Transcriptase (MMLV-RT) enzyme standard curve in dilutions that spanned the dynamic range of the assay and gave a convenient way to correlate RT activity detected in patient samples to a defined number of RT enzyme units per unit of sample. Tables 2-6 show the disease status and pool RT enzyme activity values for breast cancer, ovarian cancer and benign disease, and healthy normal donors, respectively. Figure 8 shows a representative line graph of individual fraction RT tests; fractions showing peak activity (an example is indicated by the arrow in the figure) were tested by RT-PCR. The dot plots in Figures 9-13 show the distribution of plasma RT enzyme activity test results by pool for breast cancer, ovarian cancer, benign ovarian disease, and normal donors, respectively. When patient sera and tissue isolates were tested directly for RT activity, high RFU values were seen in controls that had no RT incubation step, accounting for up to 97% of the assay signal.

	Gradient Fraction Pool RT Value					
Acc. #	A	B	C	D	Disease	+ve?
120	3146946	1234403	590791	391091	DCIS	+
127	1690669	940418	613821	535262	DCIS	+
173	959453	570692	405079	334462	DCIS	+
171	892942	1237300	593728	461829	DCIS	+
39	795948	819758	533416	467753	DCIS	+
157	687890	762709	448197	386531	DCIS	+
50	615483	533322	437016	398782	DCIS	
99	565128	395387	313325	267588	DCIS	
35	534324	514503	429078	391293	DCIS	
131	440039	410624	304537	283905	DCIS	
79	374216	681383	1106323	306653	DCIS	+
86	293832	307818	265460	227706	DCIS	
83	254463	261963	192109	176000	DCIS	
					total DCIS	13
					# DCIS positive	7
					% DCIS positive	53.8

Table 2 – Patient plasma fraction RT activity by pool and disease status - DCIS

	Gradient Fraction Pool RT Value					
Acc. #	**A**	**B**	**C**	**D**	**Disease**	**+ve?**
108	**1663377**	**698919**	**362856**	**271631**	**IDC**	**+**
147	**1444931**	**630595**	**473537**	**390047**	**IDC**	**+**
109	**1029950**	**591706**	**579065**	**443621**	**IDC**	**+**
128	**914577**	**532992**	**416109**	**368317**	**IDC**	**+**
114	**791008**	**555204**	**376870**	**306360**	**IDC**	**+**
110	**767672**	**360612**	**269517**	**236009**	**IDC**	**+**
163	**749409**	**1582853**	**1150894**	**832558**	**IDC**	**+**
45	**680608**	**510478**	**416009**	**384297**	**IDC**	
55	**677296**	**454960**	**402580**	**370610**	**DCIS+IDC**	
133	**616209**	**681671**	**414601**	**321800**	**IDC**	
28	**605161**	**649789**	**473314**	**407155**	**IDC**	
52	**591888**	**469422**	**398436**	**370830**	**IDC**	
73	**546438**	**298224**	**223078**	**194778**	**IDC**	
36	**542724**	**592988**	**454264**	**411278**	**IDC**	
155	**528752**	**1008470**	**473398**	**352257**	**IDC**	**+**
76	**525870**	**382446**	**321858**	**304557**	**ILC**	
2	**524923**	**361397**	**320211**	**290039**	**IDC**	
12	**477174**	**396590**	**343956**	**302052**	**IDC**	
48	**180754**	**154723**	**145897**	**137889**	**DCIS+tubular carcinoma**	
					total invasive cancer	**19**
					# invasive cancer positive	**8**
					% invasive cancer positive	**42.1**

Table 3 – Patient plasma fraction RT activity by pool and disease status – invasive breast cancer

	Gradient Fraction Pool					
Acc. #	**A**	**B**	**C**	**D**	**Disease**	**+ve?**
112	**1628379**	**1438226**	**1113414**	**709821**	**adenocarcinoma, IIIc**	**+**
204	**1203391**	**910734**	**564569**	**358905**	**serous adenocarcinoma**	**+**
174	**1038934**	**545113**	**338341**	**437531**	**GI stromal tumor**	**+**
65	**941650**	**784501**	**688987**	**536367**	**metastatic adenocarcinoma**	**+**
141	**701056**	**568797**	**436871**	**358138**	**endometrial adenocarcinoma**	**+**
158	**659482**	**696844**	**664830**	**513360**	**high grade ovarian carcinoma**	
105	**598699**	**770691**	**421033**	**314240**	**mullerian tumor**	**+**
67	**565812**	**1291063**	**691391**	**593853**	**high-grade serous adenocarcinoma**	**+**
125	**531077**	**521725**	**364645**	**304045**	**LMP ovarian tumor**	
115	**483775**	**695919**	**1643799**	**1880087**	**malignant mixed mullerian tumor**	**+**
153	**478361**	**428438**	**350288**	**312882**	**papillary serous**	
92	**468215**	**1140544**	**1546342**	**936441**	**papillary serous carcinoma**	**+**
					total ovarian cancer	**12**
					# ovarian cancer positive	**9**
					% ovarian cancer positive	**75**

Table 4 - Patient plasma fraction RT activity by pool and disease status – ovarian cancer

	Gradient Fraction Pool					
Acc. #	**A**	**B**	**C**	**D**	**Disease**	**+ve?**
202	**698314**	**503500**	**339894**	**290460**	**benign control**	
206	**685244**	**408884**	**297672**	**260292**	**benign cyst**	
169	**643008**	**609756**	**446303**	**319128**	**benign cyst teratoma**	
164	**602892**	**1094879**	**631250**	**458842**	**ovarian cyst**	**+**
186	**579883**	**360603**	**290234**	**253426**	**benign teratoma**	
165	**517323**	**386792**	**297022**	**255242**	**benign control**	
142	**511385**	**467847**	**421010**	**366963**	**benign cystadenofibroma**	
101	**494751**	**476209**	**323066**	**284746**	**teratoma control**	
71	**426943**	**389099**	**295179**	**258782**	**benign control**	
					total ovarian benign	**9**
					# ovarian positive	**1**
					% ovarian positive	**11.1**

Table 5 - Patient plasma fraction RT activity by pool and disease status – ovarian benign

	Gradient Fraction Pool RT Value					
Acc. #	**A**	**B**	**C**	**D**	**Disease**	**+ve?**
ND 1	**348246**	**285439**	**204213**	**181054**	**-**	
ND 4	**376103**	**318805**	**279443**	**250364**	**-**	
ND 2	**440958**	**306814**	**222697**	**165254**	**-**	
ND 6	**310911**	**884544**	**580280**	**313170**	**-**	**+**
ND 3	**641884**	**539045**	**361070**	**317444**	**-**	
ND 5	**286062**	**273739**	**277796**	**210218**	**-**	
					total normal	**6**
					# normal positive	**1**
					% normal positive	**16.67**

Table 6 – Patient plasma fraction RT activity by pool and disease status - normal

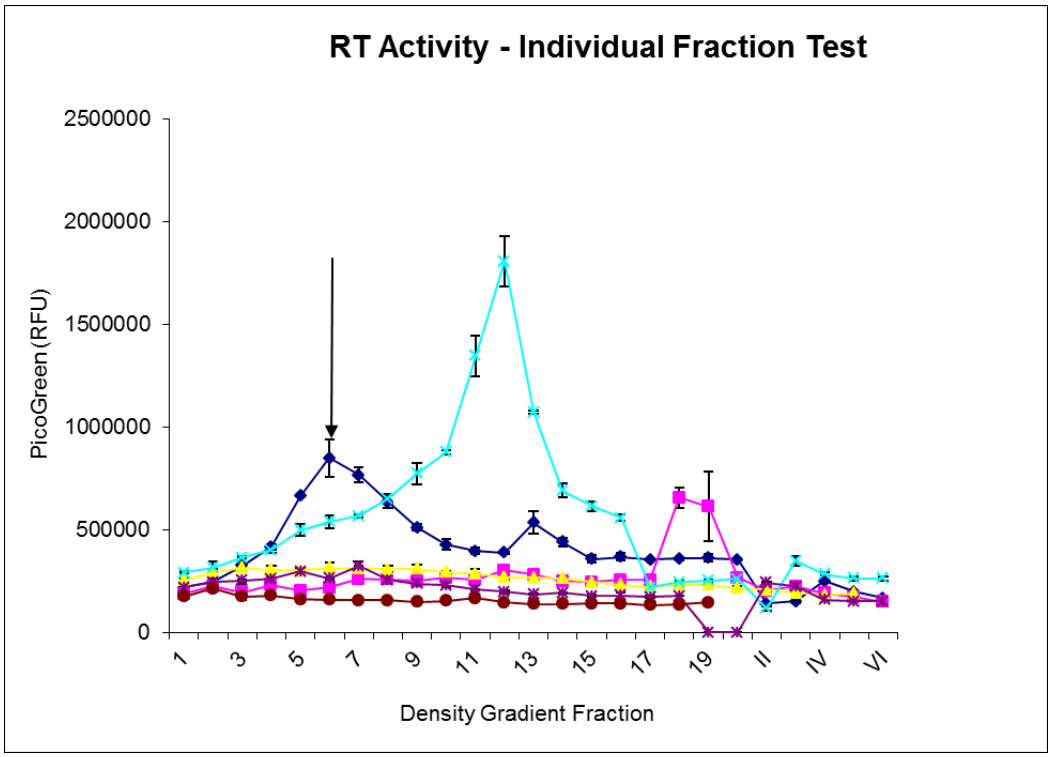

Figure 8 Individual RT activity test – Example of individual fraction RT results from both patient and normal donor plasma. Patient plasma fractions showing peak RT activity (indicated by arrow) were tested by RT-PCR using K10 and K22 primers.

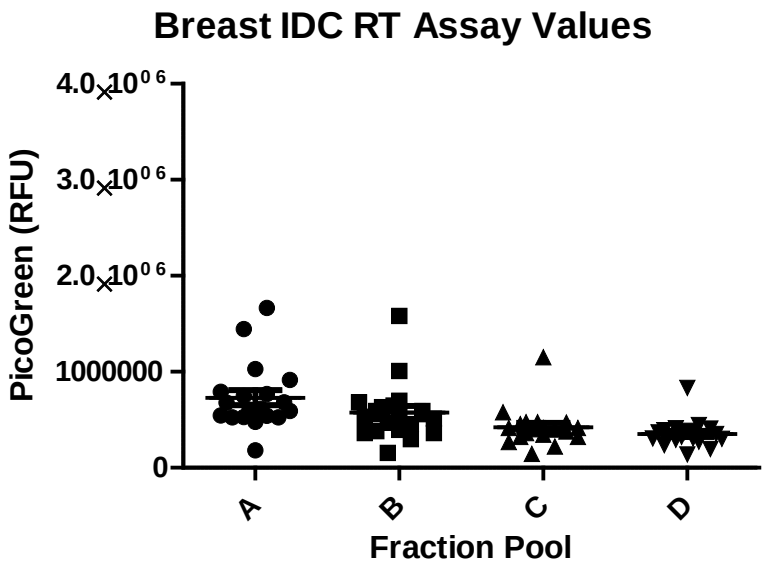

Figure 9 Dot plot of invasive breast cancer patient plasma fraction reverse transcriptase assay results by pool.

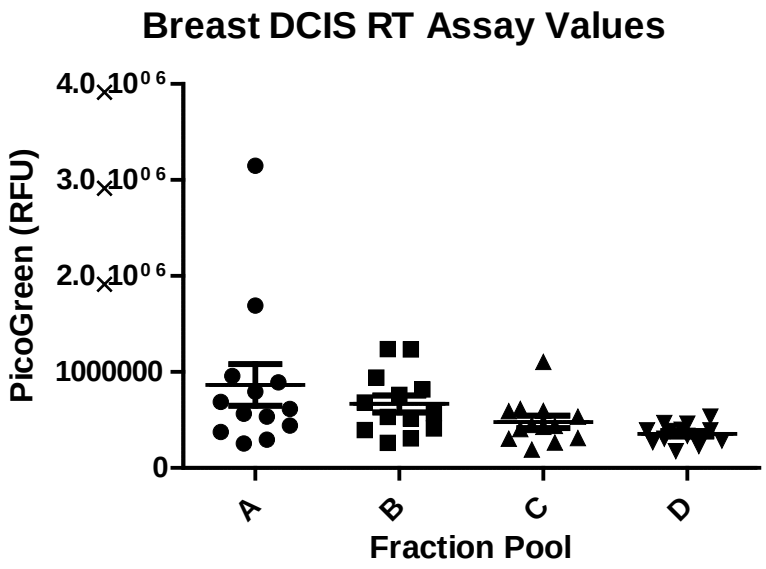

Figure 10 Dot plot of *in situ* breast cancer patient plasma fraction reverse transcriptase assay results by pool.

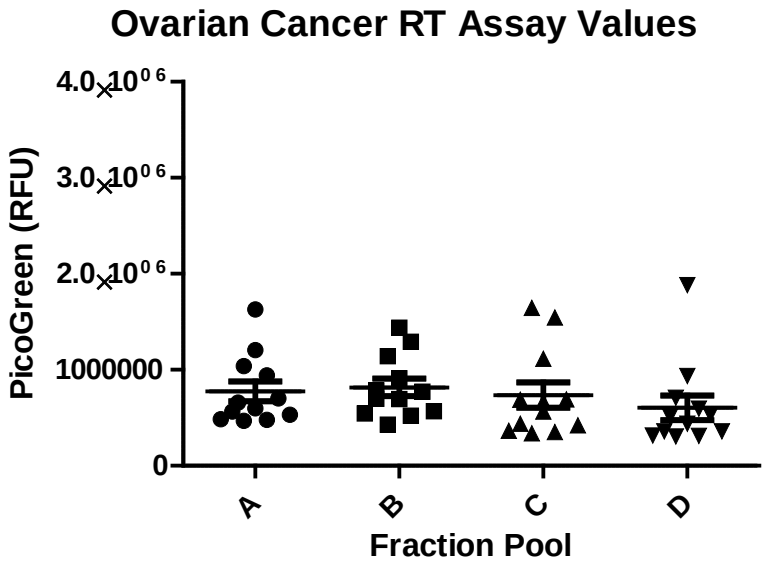

Figure 11 Dot plot of malignant ovarian disease patient plasma fraction reverse transcriptase assay results by pool.

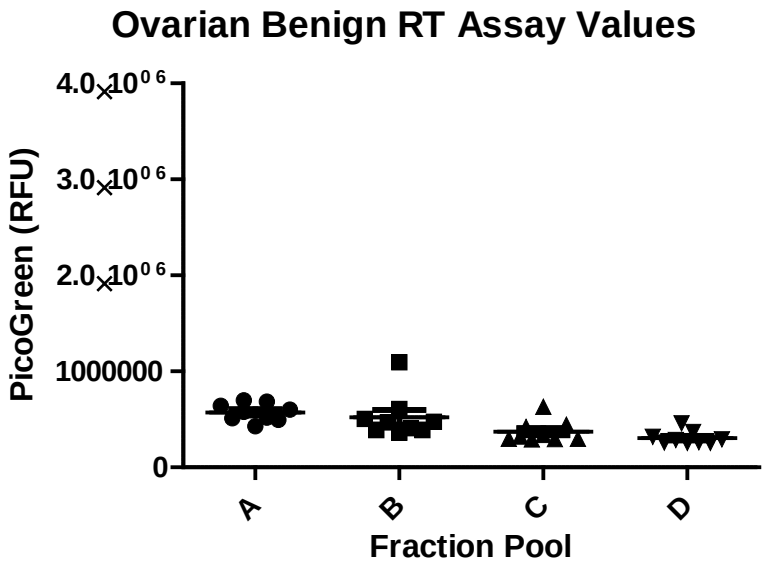

Figure 12 Dot plot of ovarian benign disease patient plasma fraction reverse transcriptase assay results by pool.

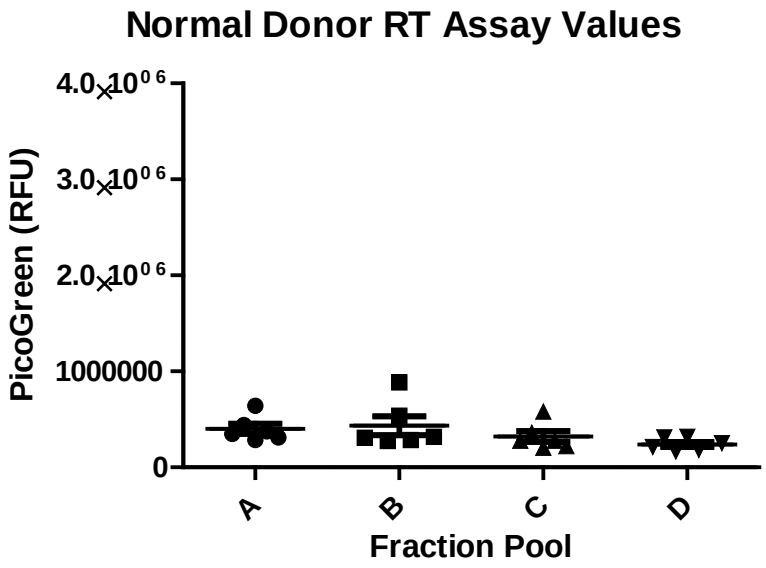

Figure 13 Dot plot of normal donor plasma fraction reverse transcriptase assay results by pool.

Because of this non-specific signal, data from direct (unfractionated) serum and tissue tests are limited in their usefulness and therefore not shown. Isopycnic fractionation was determined to be a crucial part of the sample prep to minimize background signal issues.

Select fractions showing high reverse transcriptase activity were used to isolate viral RNA and perform RT-PCR using HERV-K Env type 1 and type 2 primers, as seen in Figures 14-17. Since our vRNA template is inside of the virus, as well as the presence of heparin which interferes with downstream RT-PCR of the plasma fractions, samples were processed with Qiagen's MinElute Viral RNA kit. A sample of these RT-PCR amplicons was digested with RNase A as a control. The sample loading is as follows: amplicon from type 1 primers without RNase treatment, amplicons from type 1 primers with RNase treatment, and amplicons from type 2 primers without RNase treatment. The amplicons were resolved on 1% agarose-TAE gels, stained with ethidium bromide, and imaged. The usefulness of screening fractions for HERV-K vRNA is seriously compromised by the fact that three out of four normal donor samples that tested negative for reverse transcriptase, whose inclusion in the assay was intended as a negative control, gave amplicons with type 1 primers that could be clearly ablated with RNase treatment. Though many of the cancer patient samples also gave the proper size of amplicons using type 1 primers, this confounding result makes interpretation of RT-PCR experiments difficult, and suggests that screening for presence of HERV-K Env vRNA in plasma fractions should be accomplished by another means, such as nucleic acid sequence-based amplification (NASBA). NASBA results are not influenced by DNA contamination of the sample and use of this method would control for patient genomic DNA as a source of non-specific signal.

A.

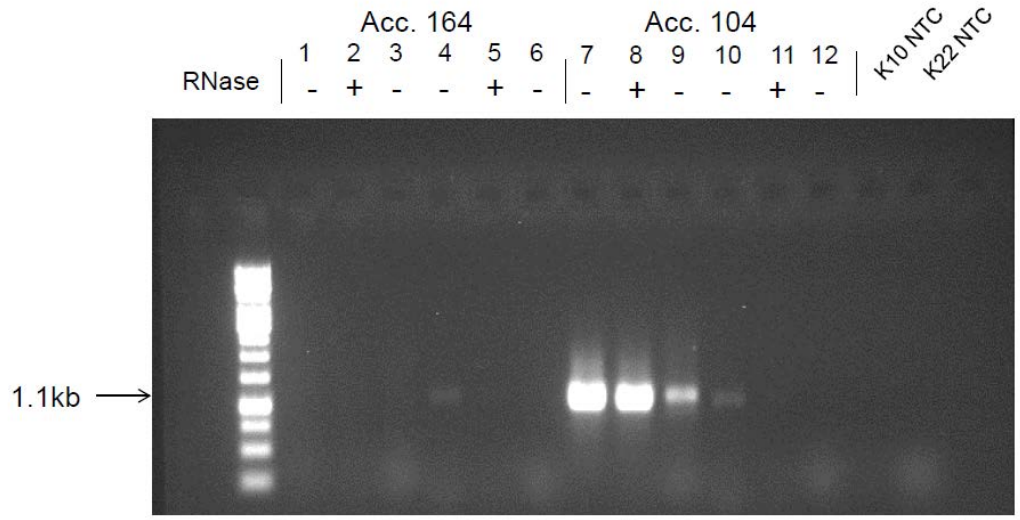

B.

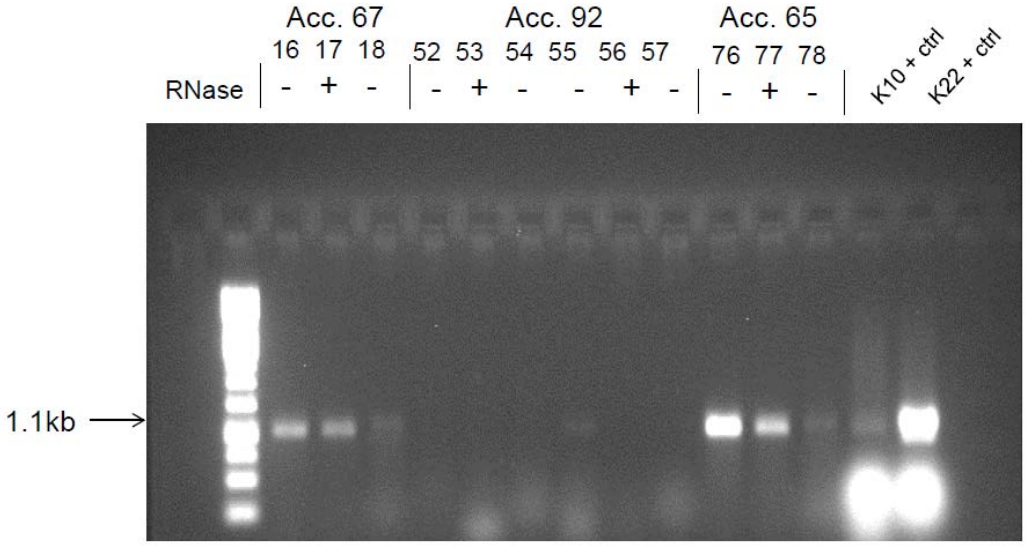

Acc. # 164 = ovarian cyst – RT+ve plasma fraction (1-3), ρ = 1.16
Acc. # 164 = ovarian cyst tissue (4-6)
Acc. # 104 = serous/ hi-grade serous ovarian carcinoma – RT+ve plasma fraction (7-9), ρ = 1.17
Acc. # 104 = serous/ hi-grade serous ovarian carcinoma – involved tumor tissue (10-12)
Acc. # 67 = high grade serous adenocarcinoma – RT+ve plasma fraction, ρ = 1.18
Acc. # 92 = papillary serous carcinoma – RT+ve plasma fractions (52-54), ρ = 1.11
Acc. # 92 = papillary serous carcinoma – involved omentum (55-57)
Acc. # 65 = metastatic adenocarcinoma – involved tumor tissue

Figure 14a, b Patient plasma fraction RT-PCR results using K10 and K22 primers.

A.

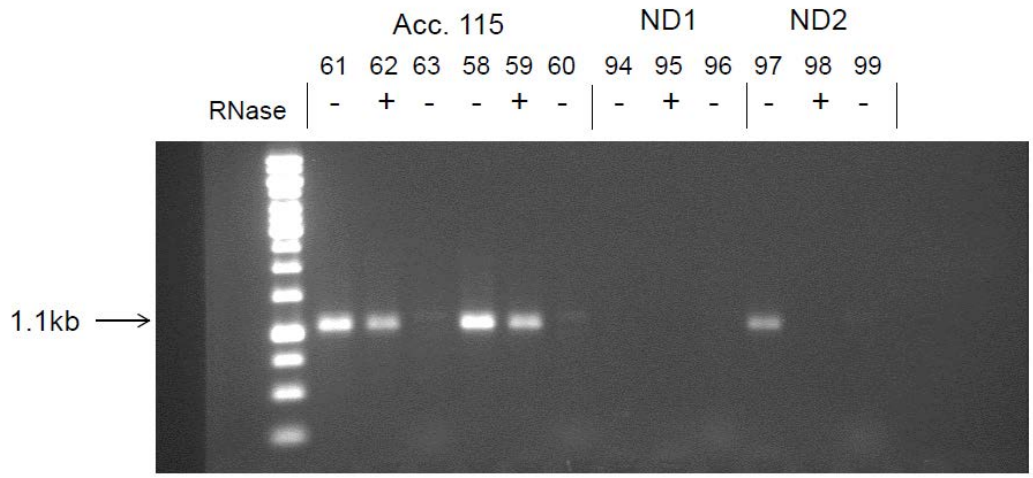

B.

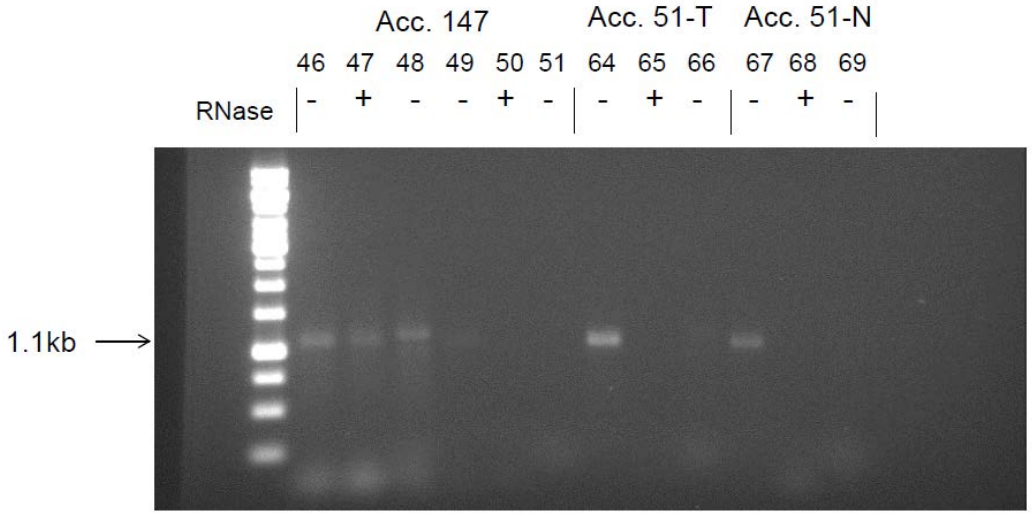

Acc. # 115 = malignant mixed mullerian tumor – RT+ve plasma fractions (2 peaks), ρ = 1.17 &1.15
ND1 = normal blood bank donor 1 – RT-ve density-matched plasma fraction ρ = 1.17
ND2 = normal blood bank donor 2 – RT-ve density-matched plasma fraction ρ = 1.17
Acc. # 147 = invasive lobular carcinoma – RT+ve plasma fraction (46-48) ρ = 1.22
Acc. # 147 = invasive lobular carcinoma – uninvolved/ adjacent tissue (49-51)
Acc. # 51-T = invasive ductal carcinoma – involved/ tumor tissue
Acc. # 51-N = invasive ductal carcinoma – uninvolved/ adjacent tissue

Figure 15a, b Patient plasma fraction RT-PCR results using K10 and K22 primers.

A.

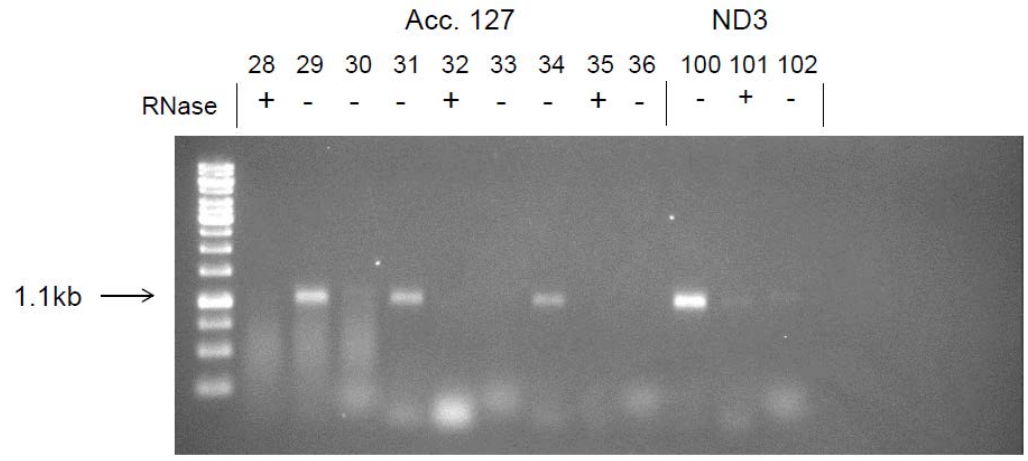

B.

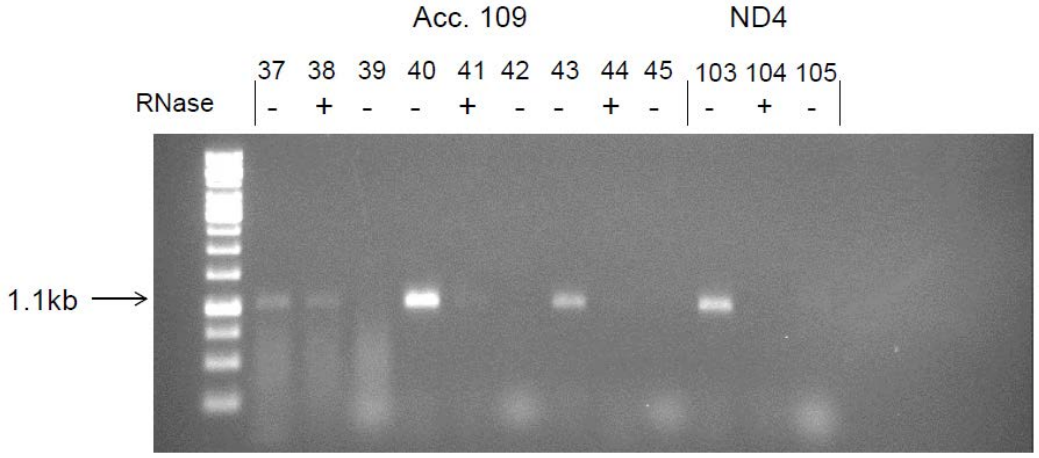

Acc. # 127 = ductal carcinoma in situ – RT +ve plasma fraction (28-30), ρ = 1.21
Acc. # 127 = ductal carcinoma in situ – involved/ tumor tissue (31-34)
Acc. # 127 = ductal carcinoma in situ – uninvolved/ adjacent tissue (34-36)
ND3 = normal blood bank donor 3 – RT-ve density-matched plasma fraction, ρ = 1.21
Acc. # 109 = invasive ductal carcinoma – RT+ve plasma fraction (37-39), ρ = 1.2
Acc. # 109 = invasive ductal carcinoma – involved/ tumor tissue (40-42)
Acc. # 109 = invasive ductal carcinoma – uninvolved/ adjacent tissue (43-45)
ND4 = normal blood bank donor 4 – RT-ve density-matched plasma fraction, ρ = 1.2

Figure 16a, b Patient plasma fraction RT-PCR results using K10 and K22 primers.

A.

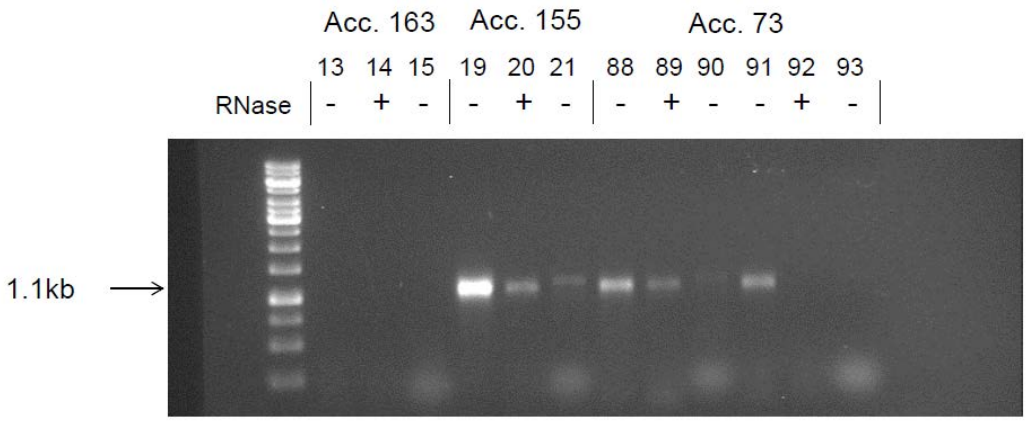

B.

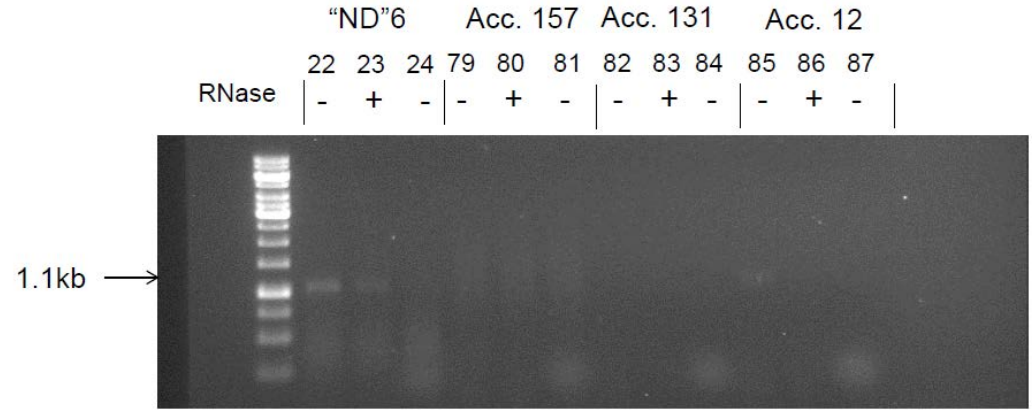

Acc. # 163 = invasive ductal carcinoma – RT+ve plasma fraction, ρ = 1.17
Acc. # 155 = invasive ductal carcinoma – RT+ve plasma fraction, ρ = 1.17
Acc. # 73 = invasive ductal carcinoma – RT+ve plasma fraction (88-90) ρ = 1.17
Acc. # 73 = invasive ductal carcinoma – involved/ tumor tissue (91-93)
"ND"6 = blood bank donor 6 – RT+ve plasma fraction, ρ = 1.11
Acc. # 157 = ductal carcinoma in situ – RT+ve plasma fraction, ρ = 1.17
Acc. # 131 = ductal carcinoma in situ – RT+ve plasma fraction, ρ = 1.17
Acc. # 12 = invasive ductal carcinoma – RT+ve plasma fraction, ρ = 1.17

Figure 17a, b Patient plasma fraction RT-PCR results using K10 and K22 primers.

From the samples that yielded an amplicon, specific bands were excised, purified, and submitted for sequencing with an HERV-K Env SU-specific primer. The reported sequences were processed by NCBI's BLAST algorithm and the results of the highest scoring alignments are shown in Table 7. Individual plasma fractions from representative patients and a normal donor were selected to test for presence of HERV-K Env SU antigen by western blotting using 6e11and anti-mouse IgG-HRP as the probe. The results from the RT activity assay and western blot along with the measured fraction density are compiled for these samples and shown in Figures 18-21.

Patient #/ Disease Status	Top Scoring BLAST Alignment	Score	E value	Acc. Number
Acc. # 104 = serous/high-grade serous carcinoma (ovarian cancer)	Human endogenous retrovirus K115	1044	0.0	AY037929.1
Acc. # 163 = invasive ductal carcinoma (IDC, breast cancer)	Homo sapiens isolate T842 endogenous virus HERV-K envelope	1450	0.0	DQ069912.1
Acc. # 155 = invasive ductal carcinoma (breast cancer)	Human endogenous retrovirus K isolate HD8.13	953	0.0	EU308984.1
Acc. # 127 = ductal carcinoma in situ (DCIS, breast cancer) with RNase treatment	Homo sapiens isolate HML-2_3q12.3 endogenous virus HERV-K	126	4e-26	JN675021.1
Acc. # 127 = DCIS	Human endogenous retrovirus K isolate HD8.5	174	2e-40	EU308977.1
Acc. # 115 = malignant mixed mullerian tumor (MMMT, ovarian cancer) peak 1	Homo sapiens isolate T842 endogenous virus HERV-K envelope	857	0.0	DQ069912.1
Acc. # 115 = MMMT (ovarian cancer) peak 2	Homo sapiens endogenous virus HERV-K chromosome 19	1426	0.0	JN656291.1
Acc. # 104 = serous/high-grade serous carcinoma (ovarian cancer)	Human endogenous retrovirus K clone 5b8	699	0.0	DQ360575.1
Sk-Br-3 (ATCC malignant breast cancer cell line, positive control)	Homo sapiens isolate HML-2_19q11 endogenous virus HERV-K	695	0.0	JN675080.1

Table 7 Top-scoring BLAST alignments from sequenced RT-PCR amplicons

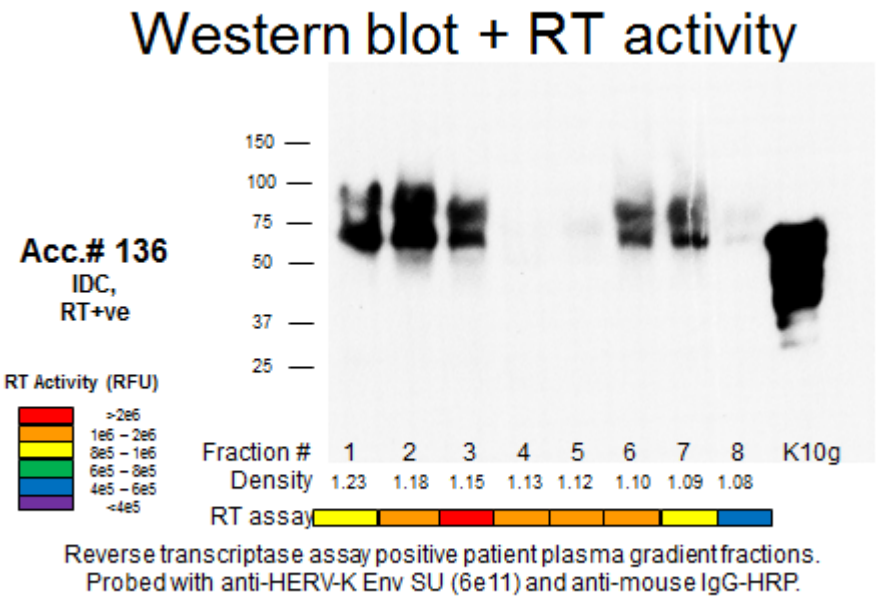

Figure 18 Patient Acc. # 136 fraction density, western blot, and RT activity.

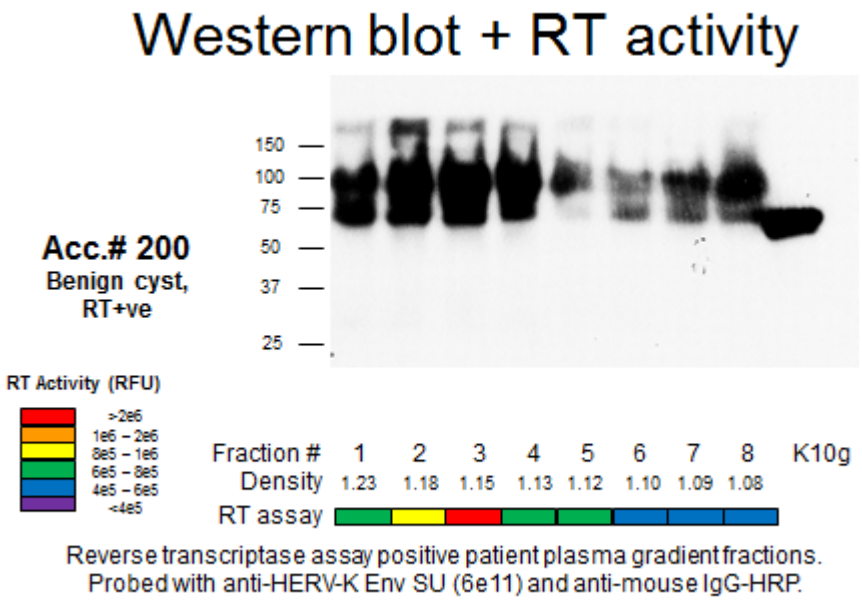

Figure 19 Patient Acc. # 200 fraction density, western blot, and RT activity.

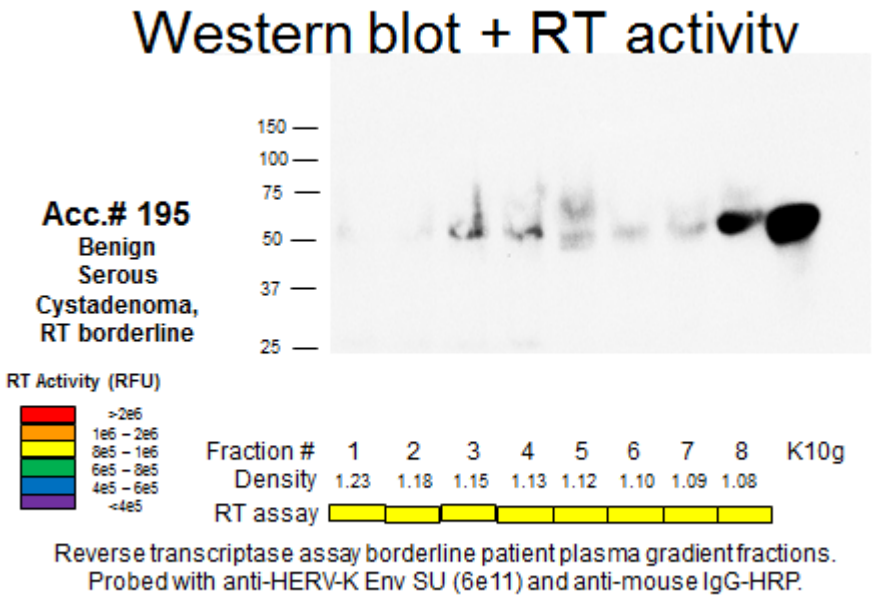

Figure 20 Patient Acc. # 195 fraction density, western blot, and RT activity.

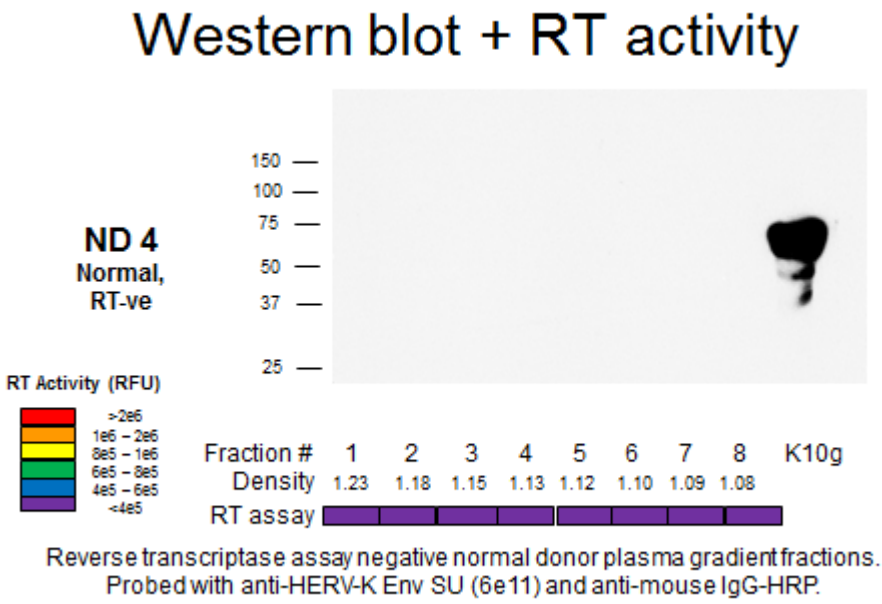

Figure 21 Normal donor #4 fraction density, western blot, and RT activity.

3.6 Anti-HERV-K Env SU Antibody Internalization Assay

In the realm of immunotherapeutics, the ability of the agent to be taken in beyond the plasma membrane is a significant benefit as it can allow loading of the target cell with various molecular cargo carried in by the internalization event, as mediated by its antibody conjugate. We tested 6e11 for its propensity to be internalized by various HERV-K Env positive and negative cell lines in culture using a standard internalization assay. HERV-K Env SU on target cell surfaces was saturated with antibody during a pre-incubation period then washed and returned to the 37° C 5% CO_2 humidified culture incubator. The cells were processed as described in materials and methods, stained with anti-mouse IgG-AlexaFluor 488, and imaged using confocal microscopy. Cells positive for HERV-K Env were able to internalize significant amounts of the 6e11 within 2 hours, whereas they did not take up the IgG2a isotype control antibody under the same conditions, as shown in Figures 22 and 23 for MDA- MB-231 and SK-BR-3, respectively. Composite tilescans covering larger areas of the slide are included to show uniformity of internalization across large numbers of cells. MCF-10AT did not take up either 6e11 or the isotype control IgG2a when prepared the same way, as shown in Figure 24. Though MCF-10AT shows intermediate HERV-K Env SU expression by western blot, the internalization result suggests the antigen is most likely confined to the cytoplasm or somehow lacks the epitope recognized by 6e11. All cell nuclei were stained with DAPI as a reference.

A.

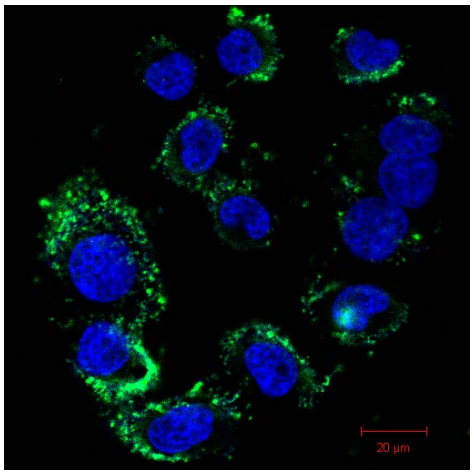

B.

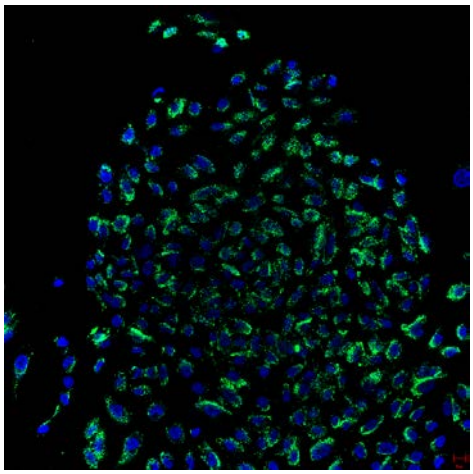

C.

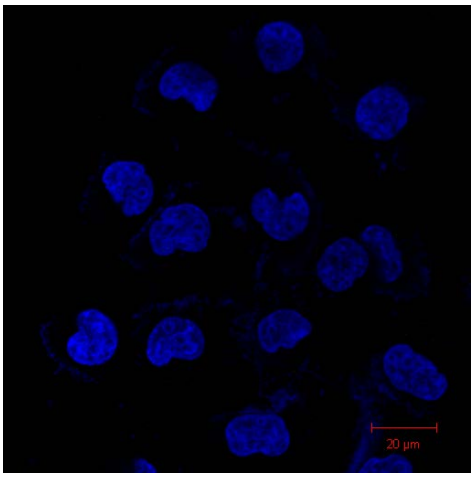

Figure 22a-c (A) Internalization of 6e11 by MDA-MB-231, single frame scan, (B) internalization of 6e11 by MDA-MB-231, 5x5 frame scans, (C) lack of internalization of isotype control IgG2a by MDA-MB-231. Scale bar = 20µm.

A. **B.**

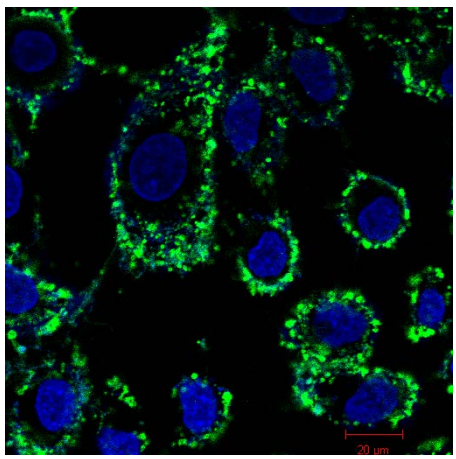

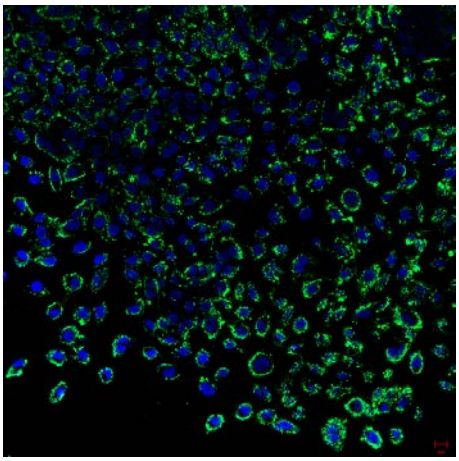

C.

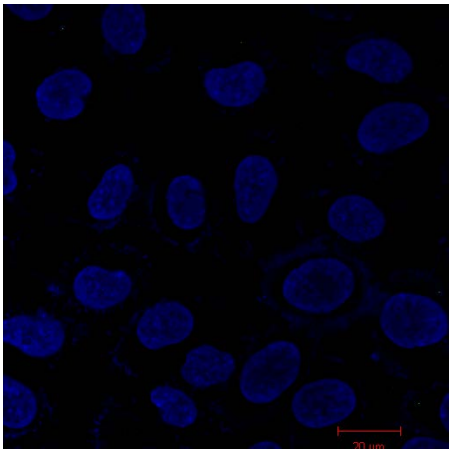

Figure 23a-c (A) Internalization of 6e11 by SK-BR-3, single frame scan, (B) internalization of 6e11 by SK-BR-3, 5x5 frame scan, (C) lack of internalization of isotype control IgG2a by SK-BR-3. Scale bar = 20µ.

A. B.

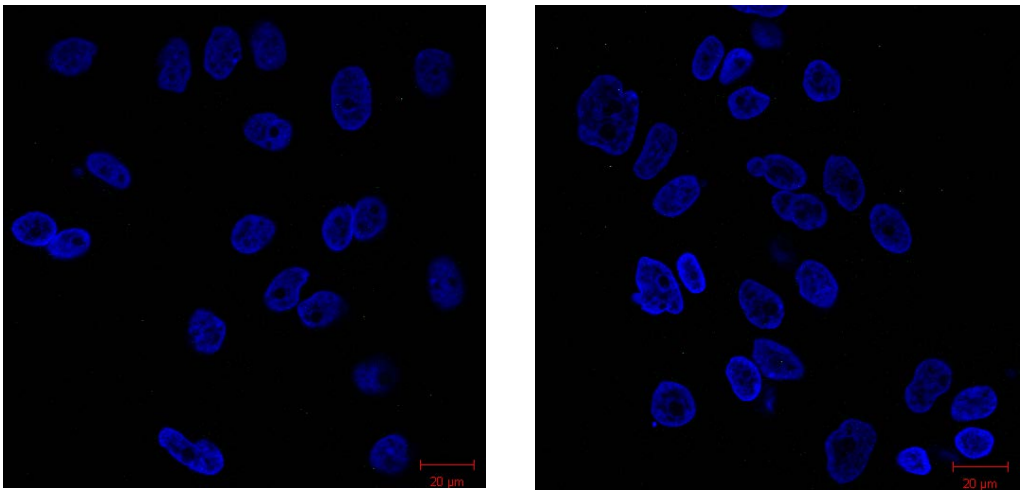

Figure 24a-b. **(**A) Lack of internalization of 6e11 by MCF-10AT, single frame scan, (B) lack of internalization of isotype control IgG2a by MCF-10AT.
Scale bar = 20µ.

3.7 Transmission electron microscopy

Three breast cancer patient plasma gradient fractions showing high reverse transcriptase activity as well as RT-PCR amplicons were imaged in an effort to detect retroviral particles. Since retroviruses, which are typically sized around a hundred nanometers in diameter, are beyond the limit of detection for visible radiation we relied on transmission electron microscopy (TEM). Carbon-coated grids were glow-discharged and diluted plasma fraction was adsorbed directly on to the grid and counterstained with uranyl acetate. In both patient samples tested, spherical nanoparticles were evident, displaying size and morphology consistent with retrovirus, as shown in Figure 25A-D and Figure 26 B. Though the size distribution of these particles was somewhat variable, most particles observed were in the 120-140 nm range and were similar in size and morphology in both patient plasma fractions. The presence of similar particles from conditioned MCF-7 media suggests that even outside of the influence of the host, cancer cells are capable of releasing virus-like particles into their surroundings that resolve to the densities reported for retrovirus using isopycnic separation techniques. These particles are shown in Figure 26 A.

TEM studies of 6h5-AuNP-dosed tumor xenografts clearly indicate the ability of our antibody to bind to the surface of and deliver cargo into HERV-K^+ cells from two different cancer types (breast and pancreatic), as indicated in Figure 26 C-F. This further illustrates the potential for our antibodies to be used as therapeutics; a tumor xenograft in a mouse is a much better drug delivery model than simple *in vitro* dosing and internalization experiments, which cannot address the complexities of pharmacokinetics. AuNP are relatively large compared to most molecules that we would plan to conjugate

A. B.

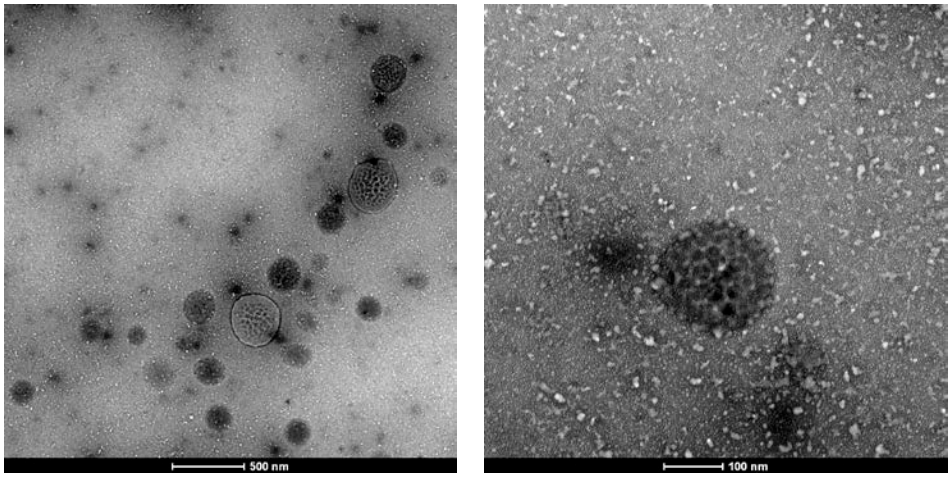

Figure 25a,b. TEM. (A) Patient 74 whole mount plasma, 26,500 x and (B) 105,000 x magnification.

C. D.

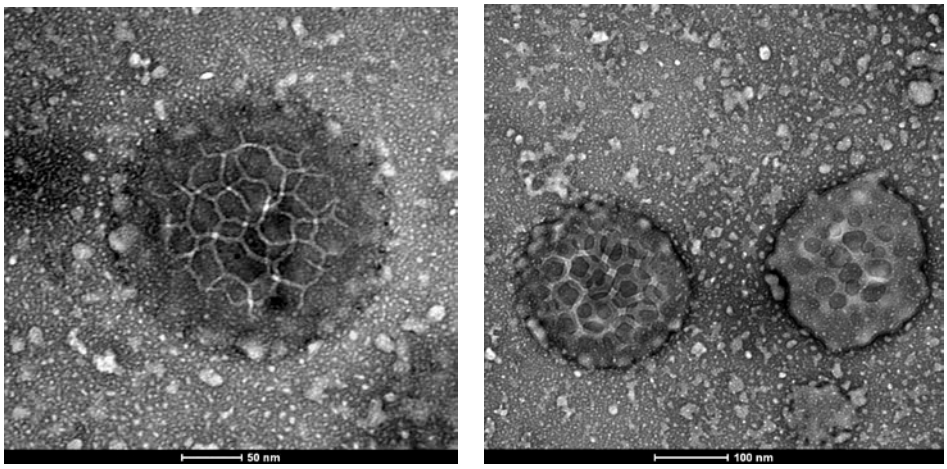

Figure 25c,d. TEM. (C) Patient 74 whole mount plasma, 220,000 x and (D) patient 75, 135,000 x magnification.

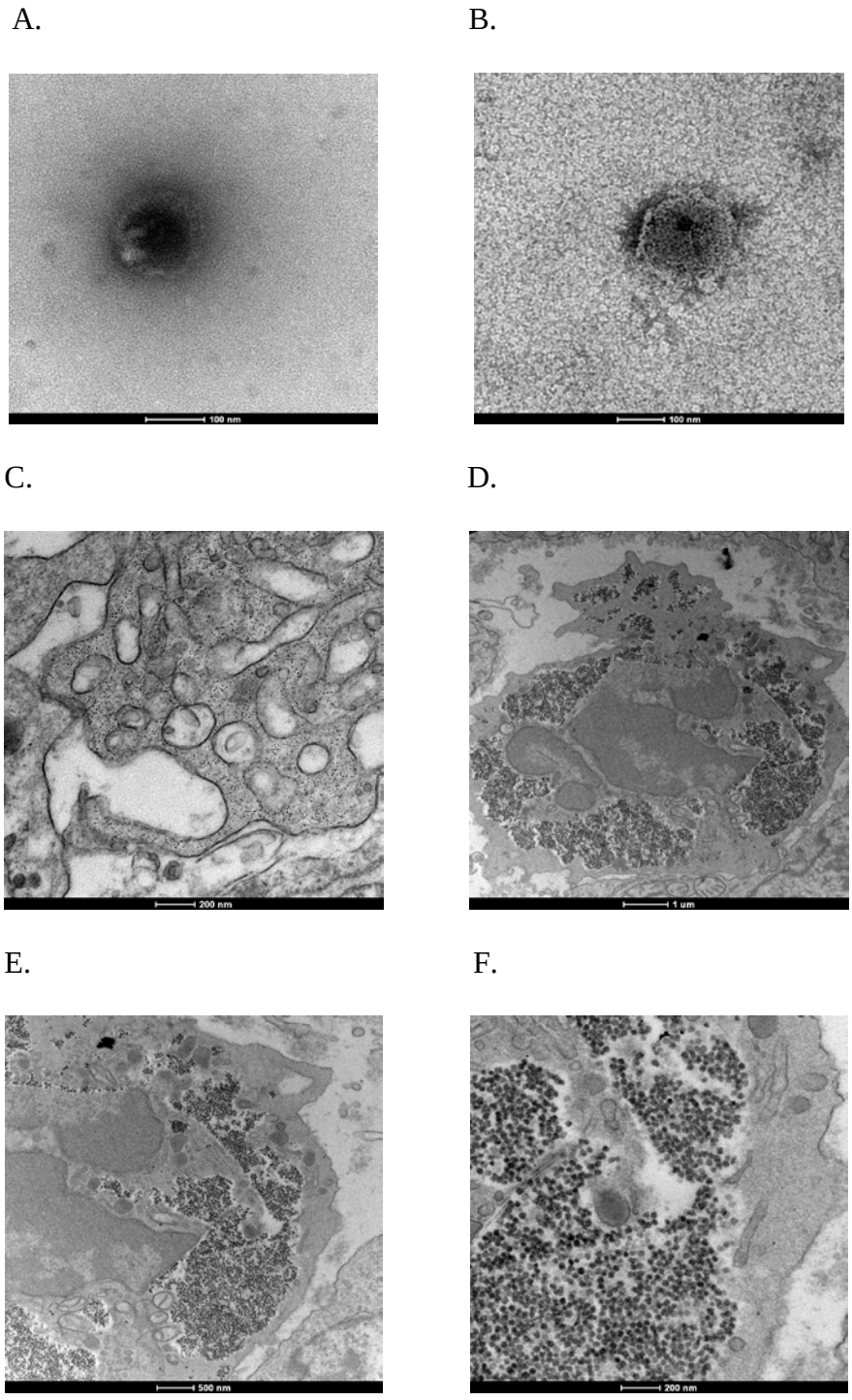

Figure 26 TEM. (A) MCF-7 confluent media fraction, 87,000 x magnification (B) Patient 78 whole mount plasma fraction, 87,000 x magnification, (C) 6h5-AuNP in MDA-MD-231 xenograft, 26,500 x magnification, (D) 6h5-AuNP in Panc-2 xenograft, 9,900 x magnification, (E) 16,500 x magnification, and (F) 43,000 x magnification.

onto the antibody (ie. antineoplastic agents and radioisotopes) so there seems to be quite a range of cargo that we could potentially deliver into HERV-K^+ cells. AuNP were chosen for this work for two reasons: 1) they are a readily seen in TEM due to their high degree of electron scattering, and 2) they can be utilized in radiofrequency thermoablation treatments to induce apoptosis in tissues containing these type of nanoparticles (28), presenting a novel therapeutic modality.

3.8 Statistical analysis of RT enzyme activity data

Patient plasma RT activity results were compared across malignant cancer patient, benign cancer patient, and normal donor samples and differences were analyzed by t-test for statistical significance. A p-value less than 0.05 was indicative of a significant difference. In invasive breast cancer plasma fractions, pool A was significantly different from normal donor pool A but no others, as seen in Figure 27. For DCIS, the only significant difference between patient and normal was found when comparing pool D values (Figure 28). The results for ovarian cancer were much more promising; significant differences could be found between 1) malignant and normal pool A, 2) malignant and normal pool B, and 3) benign and normal pool A, as shown in Figure 29. In the ovarian patients, RT activity testing was able to clearly discern samples from malignant and benign patients compared to normal donor samples, and though differences in breast plasma samples were not as pronounced, they were still present compared to normal donor plasma.

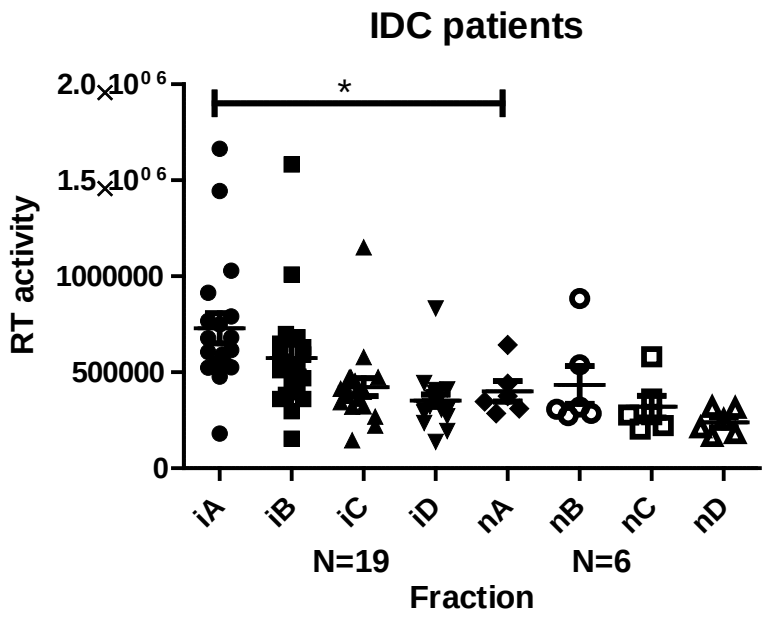

Figure 27 Patient Plasma RT assay pool value t-test for invasive breast cancer patient vs. normal donor samples.
iA-iD are invasive breast cancer patient pools and nA-nD are normal donor pools. Star indicates $p<0.05$ comparing the groups indicated.

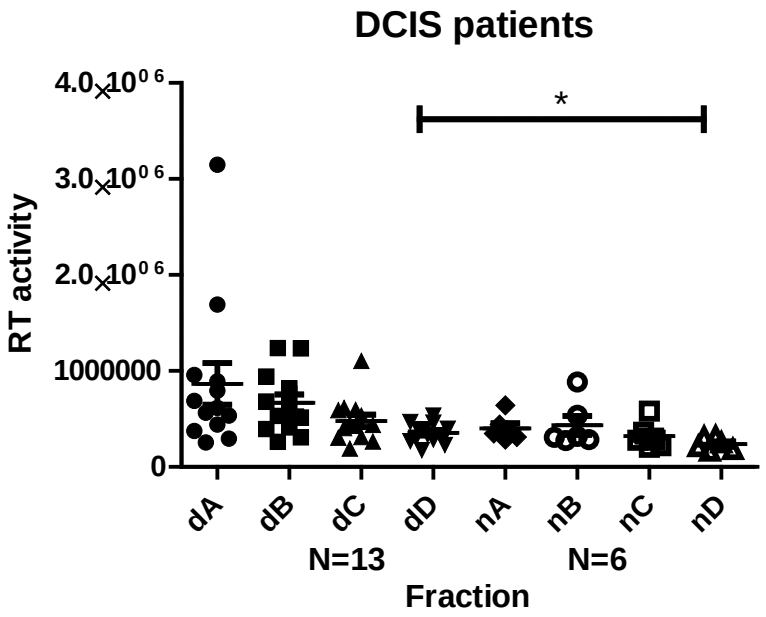

Figure 28 Patient Plasma RT assay pool value t-test for DCIS patient vs. normal donor samples. dA-dD are DCIS patient pools and nA-nD are normal patient pools. Star indicates $p<0.05$ comparing the groups indicated.

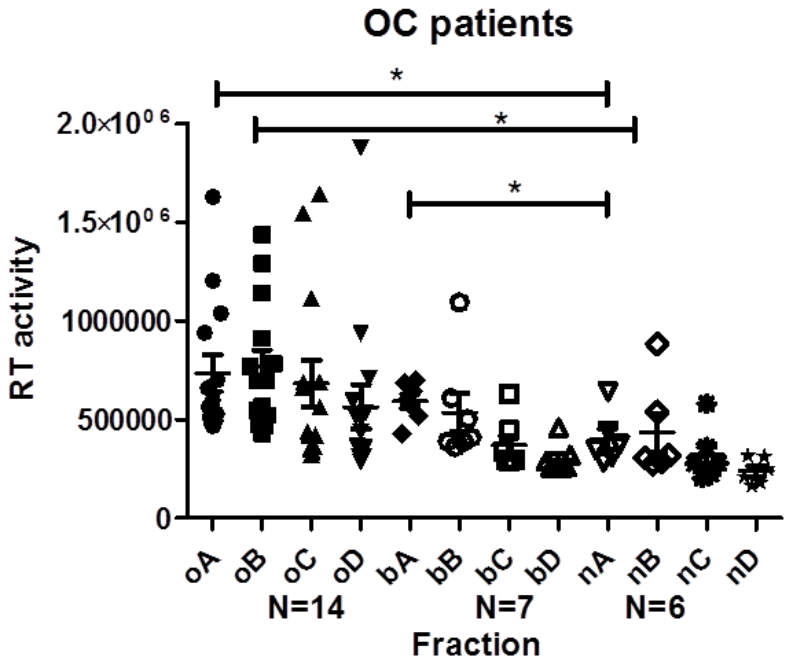

Figure 29 Patient Plasma RT assay pool value t-test for malignant and benign ovarian cancer patients compared to normal donor samples.
oA-oD are ovarian cancer plasma pools, bA-bD are benign tumor patient pools, and nA-nD are normal donor plasma pools.
Stars indicate $p<0.05$ comparing the groups indicated.

Chapter 4 Discussion

Evidence of HERV-K expression in human cancer was shown at the mRNA level over a decade ago by this lab. Upon cloning and sequencing these transcripts from various patients, it was discovered that most often multiple nonsense mutations or deletions are present, thus preventing translation of a functional viral protein and thereby excluding the possibility of functional viral particles. The full-length HERV-K Env SU mRNA that was cloned to give rise to our recombinant protein K10g was isolated from a breast cancer patient in these studies (18).

Paramount to our characterization of this emergent pathogen is a source of reasonably consistent, high affinity and specificity antibodies against viral antigens. Anti-HERV-K Env antibodies' importance as diagnostic tools for oncology was first recognized in tissue array experiments where increased intensity and distribution of IHC staining was found to correlate strongly with refractory or advanced disease, resistance to therapy, and overall poor patient prognosis (13). The high degree of sequence variation inherent among retroviruses makes targeting stable, conserved epitopes with monoclonal antibodies difficult; therefore a panel of antibodies was developed in an effort to target multiple epitopes present on the surface domain of HERV-K Env SU.

Antibody therapeutics can induce tumor cell death in a variety of ways, such as complement-dependent cytotoxicity, (CDC), antibody-dependent cell mediated cytotoxicity (ADCC) (29), targeted delivery of toxic cargo (25), receptor antagonism (30), etc. Since IgG2 antibodies show limited ability to fix complement or be recognized by immune effector cell Fc_{γ} receptors (31), a major objective for our antibodies was not only to bind to molecular targets expressed on the surface of tumors but also to be

internalized by them. This internalization event opens the possibility of delivering various molecular cargo, including nanoparticles, isotopes, and toxins, to the cytoplasm of those tumor cells for therapeutic purposes. Many highly potent toxins have been developed (gelonin and Pseudomonas exotoxin (22, 23)) which exert their influence on molecules in the cytoplasm, such as the ribosome, in order to impede vital cellular functions. Such compounds rely on surrogate cell-binding domains such as antibodies and synthetic antibody fragments to reach their intended sites of action and we look forward to forming collaborations with investigators to develop and study such compounds.

The development and studies of murine monoclonal IgGs 6h5 and 6e11 has allowed us to study the prevalence of HERV- K Env SU protein in human cancer samples as well as its distribution of expression and we hope to ultimately utilize these agents to help elucidate the role of HERV-K in human tumorigenesis. 6h5 and 6e11 were chosen as lead candidates for further study and development due to their high affinity and specificity for the HERV-K Env SU domain, thermal stability (data not shown), high active concentration, and relative ease of production at scale. Antibodies recognizing HERV-K Env SU have been used to detect its expression in patient tissue samples bearing malignant neoplasia including low- and high-grade serous adenocarcinoma, clear cell carcinoma, and low- and high-grade endometrioid cancers whereas staining patterns of cysts and normal tissue samples show little to no expression (18).

Production of our monoclonal antibodies using the ascites method was advantageous for several biological and philosophical reasons. First, we have found that

ascites fluid itself is a reasonably stable frozen storage medium from which to recover large amounts of concentrated antibody months to years after collection. Second, we also found that active antibody concentrations from ascites fluid were much higher compared to antibody purified from hybridoma culture media directly (data not shown). Also, reduced sample volumes of ascites compared to antibody purified from hybridoma culture media directly allows reduction of reagent volumes in subsequent processing steps, making the process more efficient and cost-effective. Total antibody yields from ascites aliquots were typically 1 mg final purified antibody per 1 ml of frozen ascites. Estimations of purity and activity of antibodies and synthesized molecules was determined by western blot and/ or SDS-PAGE gel staining with coomassie brilliant blue R250.

Thermodynamics of antigen:antibody interactions were evaluated using the Biacore platform. Understanding the nature of the antibody interaction with its cognate antigen is crucial; low-affinity antibodies do not typically make for good drugs since they cannot be found interacting with the antigen as often as high-affinity antibodies do. In the context of antibody-mediated drug delivery, low-affinity antibodies are less likely to be found bound to the target cell and therefore will not be internalized as readily. This becomes a bigger problem as cell surface expression of the target antigen decreases. The result is that more antibody must be used to achieve desired effect compared to a higher affinity conjugate. For diagnostic purposes, the problem is similar; more antibody must be used when working with lower affinity antibodies to get the same degree of labeling as a smaller amount of high-affinity antibody. Diagnostic tests using low affinity

antibodies are less sensitive in general and will have more issues with non-specific binding.

The antigen K10g was used as the immobilized ligand as it is the smaller of the two binding partners (67 kDa for K10g vs. 150 kDa for IgG) and allowed us to use the same sensor surfaces to evaluate all of our antigen:antibody interactions in this study. In order for the ligand immobilization to be successful, the molecule must be attracted electrostatically to the carboxymethyl dextran sensor surface to achieve concentration of ligand at the sensor surface at a pH that does not compromise the potential binding sites present on that ligand. For proteinaceous ligands, variations in unique protein pI dictate this scouting exercise; in our case 10 mM sodium acetate pH 4.5 was chosen, as it was the least acidic condition that gave satisfactory attraction to the sensor surface. Another important concern for obtaining reliable SPR data is determining sensor surface regeneration conditions. This step in the analyte injection cycle removes bound materials that are occupying binding sites on the ligand to liberate those sites to participate in analyte binding in the next injection cycle. A desirable regeneration condition is one that both 1) returns the sensor surface response to nearly the baseline response seen before the analyte injection, and 2) does not strip off or denature sufficient amounts of ligand as to render the sensor surface unstable or unusable. None of the conditions tested were effective at surface regeneration except for 10 mM sodium hydroxide, which did an excellent job of both returning the sensorgram response to baseline and preserving the fidelity of the ligand on the sensor surface. Fortunately, 6e11 was also thoroughly removed from the sensor surface using these same conditions therefore 10 mM sodium

hydroxide was the regenerant of choice for all subsequent kinetic and concentration experiments using the Biacore X100.

Kinetic evaluations were performed using Biacore on low ligand density sensor surfaces with surface densities of immobilized K10g around 200 RU. This, along with use of relatively low antibody concentrations (3 – 48 nM) and relatively high flow rates (30 µl/min) minimizes the effect of avidity when testing bivalent analytes such as IgG which can result in artificially slow off-rates, confounding affinity determinations. Our success in minimizing avidity effects experimentally is reflected by ideal χ^2 fitting statistics in all kinetic experiments. Determination of kinetic binding constants from changes in response units at the sensor surface is defined by the following equation:

$$\Delta R/\Delta T = k_a \times C \times (R_{max} - R) - k_d \times R$$

(32) where R_{max} is the maximum signal in the experiment, R is the signal for a given injection cycle, T is time, k_a is the association constant, k_d is the dissociation constant, and C is the active analyte concentration. Our kinetic data was fitted to a 1:1 (monovalent) Langmuir thermodynamic model using Biacore X100 evaluation software and the χ^2 values are at or below 1% of response maximum (R_{max}) for the assay, which is considered within the noise threshold of the instrument's detectors and has been informally adopted as a guideline for establishing goodness-of-fit of our experimental data to the binding model. The Biacore X100 evaluation software allows fitting to bivalent analyte binding models and we see little improvement of χ^2 values when fitting to these models, further indicating the 1:1 Langmuir model is appropriate. Also, in our kinetic evaluations our uniqueness value (U-value), which is a measure of

interdependence of the association and dissociation rates, was always below 10, well within the acceptable range for uniqueness.

Active (binding) concentration of purified antibody was first determined using calibration-free concentration analysis (CFCA), also on the Biacore X100 platform. This recent feature available on newer Biacore instruments with the proper analysis software allows determination of active protein concentration using a high-density ligand chip (Biacore recommends immobilization densities of 5000 to 10,000 RU). The method requires one to inject a wide range of analyte dilutions and supply a diffusion coefficient for the molecule. The instrument injects the dilution range at two different flow rates in an attempt to force mass transport limitations in the data. The derivation of thermodynamic equations describing the relationship between analyte concentration, diffusion coefficients, mass transport limitations under laminar flow, and affinity can be found in (33) for CFCA experiments and (32) for kinetic experiments. We have found that it is not uncommon for a given lot of antibody to be 50% active or less; as these errors would greatly impact the quality of the kinetic binding data, which rely on correct concentrations to produce correct kinetic constants, we have elected to employ CFCA data to determine active antibody concentration for further kinetic experiments on these molecules.

Western blotting results of cultured malignant and control cells lines probed for HERV-K Env SU shows very nice correlation between disease state and HERV-K Env expression levels. In support of our hypothesis, all breast cancer cell lines tested were positive for HERV-K Env. The benign cell line MCF-10A was negative for HERV-K Env and the H-Ras-transformed benign cell line MCF-10AT showed an intermediate

expression level of HERV-K Env between cells derived from benign and malignant cancer tissue.

Patient plasma density gradient fractions were pooled and analyzed by a microplate-based reverse transcriptase enzyme activity assay EnzChek RT (Invitrogen). This system relies on reverse transcriptase activity in the sample to synthesize RNA:DNA heteroduplexes from a pre-annealed poly (A) RNA template and oligo dT primer. The reaction products are stained with PicoGreen, a dye that is highly specific for duplex nucleic acids. The fluorescence spectra of PicoGreen:duplex nucleic acid show excitation and emission maxima at 503 nm and 522 nm, respectively. Since many biological samples will show autofluorescence using these excitation and emission wavelengths, the plates were read on the reader before and after the addition of the reporter dye. A low baseline autofluorescence was noted from all plasma fractions that corresponded approximately to the amount of signal seen in reverse transcriptase negative normal donor plasma. Isopycnic density gradient fractionation of plasma was able to resolve viral particles from bulk plasma impurities and gave useful results; this was not the case for patient tissue isolates. Because the tissue was disrupted, clarified, and sampled directly without density fractionation, much larger amounts of either genomic DNA, autofluorescent debris, or both, were present in the sample. In tissue isolates, the majority of the reverse transcriptase assay signal could be realized without carrying out the actual RT incubation step. This was also the case when patient sera were assayed directly (without density fractionation) with this same method; up to 97% of the reverse transcriptase assay signal was realized without carrying out the RT incubation step (data not shown). Of course, this is somewhat less of an issue when samples derived

in the same way are compared to one another, for example when comparing tumor and uninvolved tissue from the same patient, but significant confounding biases can still exist. For example, uninvolved tissue from beyond the tumor margin may not have the same composition or distribution of cell and tissue types as the neoplastic sample. The malignant tissues may also have differences in tissue concentrations of autofluorescent compounds or possibly DNA content due to hyperploidy of malignant cells. As a result, plasma fraction RT activity results cannot be readily compared to either tissue homogenate or serum direct test values. Comparison and statistical analysis of patient and normal donor plasma fraction RT activity values, however, showed statistical significance by t-test ($p<0.05$) in all patient groups. Once much larger patient populations of breast, ovarian, as well as other cancer patient plasma can be screened for RT activity to verify that these findings extend beyond the scope of this study, reverse transcriptase enzyme activity could become a bona fide screening tool to determine or predict patient disease state.

Reverse Transcription - Polymerase Chain Reaction was carried out on a sampling of patient plasma density gradient fractions showing high RT activity. These patients represent several different gynecological cancers, including malignant breast neoplasia such as ductal carcinoma *in situ* (DCIS), invasive ductal carcinoma (IDC), and invasive lobular carcinoma (ILC). Malignant ovarian cancer types including serous and high-grade serous adenocarcinoma, papillary serous carcinoma, malignant mixed mullerian tumor (MMMT), and metastatic adenocarcinoma were also assayed. For control purposes, we included samples from several patients bearing benign ovarian disease as well as numerous healthy blood bank donors. Since we are attempting to

amplify intronless retroviral elements, our primers will generate an amplicon of identical size from either genomic DNA (from the host) or vRNA templates. Qiagen's One-Step RT-PCR kit was chosen for its ability to specifically amplify very small amounts of template efficiently using a cocktail of polymerases and its high degree of sensitivity, down to 1 pg of template. With this system, cDNA is also generated in a sequence-specific manner, minimizing the number of extraneous templates that could interfere with the assay. One drawback, however, is that the entire process occurs in a single tube in continuous fashion, precluding the opportunity to run a parallel control omitting the RT reaction in the same system. In the large-scale RT-PCR screen, we chose to include RNase A-digested vRNA template control in an attempt to account and control for genomic DNA contamination in the sample. In this case, the digested template will show ablation of the amplicon, indicating that the template was indeed RNA. If the after RNase A digestion the amplicons prevails, the template was most likely host genomic DNA. We performed a similar control using DNase I to digest possible host genomic DNA in fractions before RT-PCR, however difficulties in deactivating the enzyme lead to inhibition of the subsequent RT-PCR. Samples that show amplicons at the correct molecular weight were excised and submitted for sequencing; sequencing results were aligned to sequences deposited in PubMed using BLAST. A useful exercise would be to identify open reading frames, mutations, and stop codons in the translated sequences and compare findings between cancer patient, benign tumor patient, and normal samples; more information can surely be extracted from these comparisons.

Western blotting of patient plasma gradient fractions posed unique challenges due to the presence of iodixanol density gradient media as well as high concentrations of

plasma protein, especially in the most dense samples, along with blood lipids. The problem became apparent after heating in standard Laemmli reducing sample buffer, where many times the sample would turn into either a gel or semi-solid form. Even with increasing amounts reducing sample buffer, smearing of the samples on the blot was an issue in preliminary attempts. After some testing, a sample buffer containing adequate amounts of chaotrope, detergent, and reducing agent to keep the sample fully solubilized was chosen. The final sample buffer recipe containing 6 M urea, 1% CHAPS, 2% SDS, and 50 mM DTT was employed. Blots were probed with 6e11 primary and anti-mouse IgG-HRP secondary antibodies. An enhanced chemiluminescent HRP substrate (Western Lightening Plus, Perkin Elmer) was used to develop the blots and light emission was captured in a dark room using BioMax Light blue-sensitive double emulsion ECL imaging film at multiple exposure times. A lane containing recombinant K10g was included to ascertain antibody binding specificity as was a lane of molecular weight standard (Precision Plus Kaleidoscope, Bio-Rad). Bands corresponding to HERV-K Env SU were detected in lanes where fraction density matched that reported for retrovirus, around 1.18. Western blot data, reverse transcriptase activity, and fraction density were in very good agreement for all patients tested.

An antibody internalization assay was carried out in order to determine our monoclonal antibodies' potential for binding to and delivering various molecular cargo into cells expressing HERV-K Env on their cell surface. Use of mountants with relatively high, matched indices of refraction help to minimize spherical aberrations in the image; pure glycerol has an index of refraction around 1.47, closely matching that of the coverglass and immersion oil used (borosilicate glass = 1.51 and Zeiss Immersol

518F = 1.52). In order to acquire confocal images, detection pinhole apertures for each channel were set at 1 airy unit, an optimal diameter for best image signal-to-noise ratio and an ideal compromise between resolution and signal intensity. At 1 airy unit the diameter of the emission pinhole matches that of the airy disk generated by diffraction of the point light source originating within the sample and the actual 1 airy unit diameter of the pinhole is determined by the wavelength of the diffracted radiation and the numerical aperture of optical components in the microscope. Based on Rayleigh's criterion, the critical determinant of the scale at which features can be spatially resolved is determined largely by the wavelength of radiation used in the imaging process. For circular apertures the maximum theoretical resolution using visible radiation (using 550 nm average λ for visible radiation) is around 275 nm, much greater than the size of our virus. In order to directly visualize viral particles from patient plasma density gradient fractions, we utilized transmission electron microscopy (TEM).

Betaretroviral particles have been reported in previous efforts to be at or around 100 nm in diameter (14). TEM can generate an electron beam at 80 kv acceleration with sufficiently short wavelength to readily image structures at nanometer scale, well within the range of our virus. In retrospect, early attempts at adsorbing viral particles onto carbon-coated grids were probably futile, since the carbon layer is hydrophobic and would not tend to bind materials whose nature is hydrophilic. Consultation with an expert in the field (Dr. Dwight Romanovicz, University of Texas at Austin Institute of Cellular and Molecular Biology Microscopy Core) lead to the notion of glow-discharging the carbon layer to impart upon it a temporary charge. Immediately after the glow discharge treatment the diluted plasma fraction was adsorbed and counterstained; it

was this processing that allowed us to capture images of a nanoparticle with size, staining, and morphology similar to that reported for retrovirus. That these particles were identified in cancer patient density gradient fractionated plasma samples with high reverse transcriptase activity, RT-PCR amplicons for HERV-K Env SU, and density equal to that reported for retrovirus, lends credence to the notion that these nanoparticles are indeed HERV-K. At lower magnifications, the relative abundance of particles can be seen. There appears to be range of sizes, suggesting varying degrees of virus maturity in the same patient.

TEM images of immune-compromised mice bearing xenograft tumors dosed with 6h5-AuNP show internalization of large amounts of AuNP into those tissues. Tumor-bearing mice are a significant improvement over *in vitro* dosing experiments as the distribution, metabolism, and elimination aspects of pharmacokinetics are in effect much as they would be in an actual patient in the clinic. Abnormalities in tumor vasculature play a major role in the uptake and retention of drugs and nanoparticles and it gives us great hope for the potential of anti-HERV-K Env SU-binding antibodies and their conjugates as therapeutics to see such robust delivery of materials to HERV-K^+ cell types. These data were generated for demonstrative purposes only in a pilot study; further work will need to be done with isotype control antibody-AuNP conjugates and AuNP only to check for non-targeted uptake of AuNP into HERV-K^+ tissues. The pilot study also included HERV-K^+ pancreatic cancer, which is why this cancer type was included in a text focusing on breast and ovarian cancers, but the results were excellent and warrant further studies carried out with the proper controls mentioned above.

Chapter 5 Conclusion and Further Studies

5.1 Conclusion

Profiling patient and donor sample reverse transcriptase activity proved to be useful marker for determining patient disease status, especially for ovarian cancers. Confirmation of the presence of plasma reverse transcriptase activity can be used to predict disease, though absence of activity is somewhat indeterminate.

Our antibodies recognizing HERV-K Env SU domain show great promise as both diagnostic and therapeutic agents in oncology. Their high specificity and sensitivity for HERV-K Env SU make them excellent candidate diagnostic tools and their propensity for internalization into tumor cells expressing HERV-K Env on their surface make them attractive candidates for further developmental efforts.

5.2 Future Studies

A survey of patient plasma sample reverse transcriptase activity from other cancer types, such a melanoma, hepatic, pancreatic, and lung cancer, would be useful to determine how broadly-applicable this screening strategy would be for other disease types. Thorough pre-screening of patients for viral pathogens would be highly advantageous to minimize confounding results related to the possible presence of viruses that are not HERV-K.

Cloning, humanization, and affinity maturation of our murine anti-HERV-K Env SU binding sequences could enable the development of first-in-class immunotherapeutics. Conjugation of these engineered antibodies to chemotherapy agents, prodrugs, radioisotopes, fluorescent dyes, toxin fragments, or enzymes would only increase the utility and potential of these molecules in the laboratory and clinic.

Bibliography

1. Rous, P: A transmissible avian neoplasm. (Sarcoma of the common fowl.). Journal of Experimental Medicine 12(5): 696-705, 1910.

2. Shope RE and Hurst EW: Infectious papillomatosis of rabbits: with a note on the histopathology. Journal of Experimental Medicine 31;58(5): 607-24, 1933.

3. Bittner JJ: Some possible effects of nursing on the mammary gland tumor incidence in mice. Science 84(2172): 162, 1936.

4. Spandidos DA and Anderson MLM: Oncogenes and onco-suppressor genes: their involvement in cancer. Journal of Pathology 157: 1-10, 1989.

5. McLaughlin-Drubin ME and Munger K: Viruses associated with human cancer. Biochim Biophys Acta 1782: 127-50, 2008.

6. Sarid R and Gao SJ: Viruses and human cancer: from detection to causality. Cancer Letters 305: 218-27, 2011.

7. Li WH, Gu Z, Wang H, Nekrutenko A: Evolutionary analysis of the human genome. Nature 409: 847-849, 2001.

8. Fuchs NV, Kraft M, Tondera C, Hanschmann KM, Löwer J, and Löwer R: Expression of the human endogenous retrovirus group HML-2/HERV-K does not depend on canonical promoter elements but is regulated by transcription factors Sp1 and Sp3. Journal of Virology 85 (7): 3436-48, 2011.

9. Lee YN, Malim MH, and Bieniasz PD: Hypermutation of an ancient human retrovirus by APOBEC3G. Journal of Virology 82(17): 8762-70, 2008.

10. Villesen P, Aagaard L, Wiuf C, and Pedersen FS: Identification of endogenous retroviral reading frames in the human genome. Retrovirology 1: 32, 2004.

11. Li MD, Bronson DL, Lemke TD, and Faras AJ. Restricted expression of new HERV-K members in human teratocarcinoma cells. Virology 208: 733-41, 1995.

12. Yolken RH, Karlsson H, Yee F, Johnston-Wilson NL, and Torrey EF: Endogenous retroviruses and schizophrenia. Brain Research Reviews 31: 193-99, 2000.

13. Wang-Johanning F, Liu J, Rycaj K, Huang M, Tsai K, Rosen DG, Chen DT, Lu DW, Barnhart KF, and Johanning GL: Expression of multiple human endogenous retrovirus surface proteins in ovarian cancer. International Journal of Cancer 120: 81-90, 2007.

14. Al-Allaf FA, Coutelle C, Waddington SN, David, AL Harbottle R and Themis M: LDLR-Gene therapy for familial hypercholesterolemia: problems, progress, and perspectives. International Archives of Medicine 3: 36, 2010.

15. Jern P, Sperber GO and Blomberg J: Use of endogenous retroviral sequences (ERVs) and structural markers for retroviral phylogenetic inference and taxonomy. Retrovirology 2: 50, 2005.

16. Bannert N, Kurth R: Retroelements and the human genome: new perspectives on an old relation. Proceedings of the National Academy of Science USA 101: 14572-79, 2004.

17. International Agency for Research on Cancer (IARC) Section of Cancer Information: Globocan 2008. http://globocan.iarc.fr/factsheets/populations/factsheet.asp?uno=900.

18. Wang-Johanning F, Frost AR, Johanning GL, Khazaeli MB, LoBuglio AF, Shaw DR and Strong TV: Expression of human endogenous retrovirus transcripts in human breast cancer. Clinical Cancer Research 7: 1553-60, 2001.

19. Wang-Johanning F, Radvanyi L, Rycaj K, Plummer JB, Yan P, Sastry KJ, Piyathilake CJ, Hunt KK and Johanning GL: Human endogenous retrovirus K triggers an antigen-specific immune response in breast cancer patients. Cancer Research 68: 5869-77, 2008.

20. Seifarth W, Baust C, Murr A, Skladny H, Krieg-Schneider F, Blusch J, Werner T, Hehlmann R, and Leib-Mosch C: Proviral structure, chromosomal location, and expression of HERV-K-T47D, a novel human endogenous retrovirus derived from T47D particles. Journal of Virology 72: 8384-91, 1998.

21. Contreras-Galindo R, Kaplan MH, Leissner P, Verjat T, Ferlenghi I, Bagnoli F, Giusti F, Dosik MH, Hayes DF, Gitlin SD and Markovitz DM: Human endogenous retrovirus K (HML-2) elements in the plasma of people with lymphoma and breast cancer. Journal of Virology 82: 9329-36, 2008.

22. Pai LH, Batra JK, Fitzgerald DJ, Willingham MC, Pastan I: Anti-tumor activities of immunotoxins made of monoclonal antibody B3 and various forms of Pseudomonas exotoxin. Proceeding of the National Academy of Science USA 88(8): 3358-62, 1991.

23. Dean A, Talpaz M, Kantarjian H, Faderl S, Jabbour E, Ravandi Kashani F, O'Brien SM, Rosenblum M, Cortes JE: Phase I clinical trial of the anti-CD33 immunotoxin HuM195/rgel in patients (pts) with advanced myeloid malignancies. Journal of Clinical Oncology ASCO Annual Meeting Proceedings (Post-Meeting Edition) 28;5: 6549, 2010.

24. Wiseman GA, White CA, Stabin M, Dunn WL, Erwin W, Dahlbom M, Raubitschek A, Karvelis K, Schulthiess T, Witzig TE, Belanger R, Spies S, Silverman DHS, Berlfein JR, Ding E, and Grillo-Lopez AJ: Phase I/II ^{90}Y-Zevalin (yttrium-90

ibritumomab tiuxetan, IDEC-Y2B8) radioimmunotherapy dosimetry results in relapsed or refractory non-Hodgkin's lymphoma. European Journal of Nuclear Medicine 27: 766-77, 2000.

25. Krop IE, Beeram M, Modi S, Jones SF, Holden SN, Yu W, Girish S, Tibbitts J, Yi JH, Sliwkowski MX, Jaconson F, Lutzker SG, Burris HA: Phase I study of trastuzumab-DM1, an HER2 antibody-drug conjugate, given every 3 weeks to patients with HER2-positive metastatic breast cancer. Journal of Clinical Oncology 28;16: 2698-2704, 2010.

26. Francis RJ, Sharma SK, Springer C, Green AJ, Hope-Stone LD, Sena L, Martin J, Adamson KL, Robbins A, Gumbrell L, O'Malley D, Tsiompanou E, Shahbakti H, Webley S, Hochhauser D, Hilson AJ, Blakey D, and Begent RHJ: A phase I trial of antibody directed enzyme prodrug therapy (ADEPT) in patients with advanced colorectal carcinoma or other CEA producing tumours. British Journal of Cancer 87: 600-07, 2002.

27. Wang-Johanning F, Rycaj K, Plummer JB, Li M, Yin B, Frerich K, Garza J, Shen JJ, Lin K, Yan P, Glynn SA, Dorsey TH, Hunt KK, Ambs S and Johanning GL: Immunotherapeutic potential of anti-human endogenous retrovirus-K envelope protein antibodies in targeting breast tumors. Journal National Cancer Institute 104;3: 189-210, 2012.

28. Gannon CJ, Patra CR, Bhattacharya R, Mukherjee P, and Curley S: Intracellular gold nanoparticles enhance non-invasive radiofrequency thermal destruction of human gastrointestinal cancer cells. Journal of Nanobiotechnology 6: 2, 2008.

29. Natsume A, Niwa R, Satoh M: Improving effector functions of antibodies for cancer treatment: enhancing ADCC and CDC. Drug Design, Development, and Therapy 3: 7-16, 2009.

30. Wu Y, Zhong Z, Huber J, Bassi R, Finnerty B, Corcoran E, Li H, Navarro E, Balderes P, Jimenez X, Koo H, Mangalampali VRM, Ludwig D, Tonra JR, and Hicklin DJ: Anti-vascular endothelial growth factor receptor-1 antagonist antibody as a therapeutic agent for cancer. Clinical Cancer Research 12(21): 6573-84, 2006.

31. Lefranc MP and Lefranc G: The Immunoglobulin FactsBook. Academic Press: 2001.

32. Karlsson R, Michaelsson A, Mattsson L: Kinetic analysis if monoclonal antibody-antigen interactions with a new biosensor based analytical system. Journal of Immunological Methods 145: 229-240, 1991.

33. Christensen LLH: Theoretical analysis of protein concentration determination using biosensor technology under conditions of partial mass transport limitation. Analytical Biochemistry 249: 153-164, 1997.

Vita

Joshua Brandon Plummer was born in Austin, Texas, USA on December 27, 1979, the son of Charles Earnest and Donna Nawara Plummer. Upon graduation from Bastrop High School, Bastrop, Texas, USA, he matriculated to The University of Texas at Austin. He earned a Bachelor of Science in Biology with an emphasis on cellular and molecular biology in May, 2005. Upon graduation he began work at University of Texas M. D. Anderson Cancer Center – Keeling Center for Comparative Medicine, first as an entry-level research assistant and currently holds the position of research laboratory coordinator. In January, 2009 he entered The University of Texas Health Science Center at Houston Graduate School of Biomedical Sciences to pursue a Master of Science in Experimental Therapeutics.

Permanent Address:

13608 Gilwell Drive

Del Valle, Texas 78617

USA